SOLAR-C Interim Report:

SOLAR-C Plan-A

A Direct Approach to the Origin of the Solar Activity Cycle

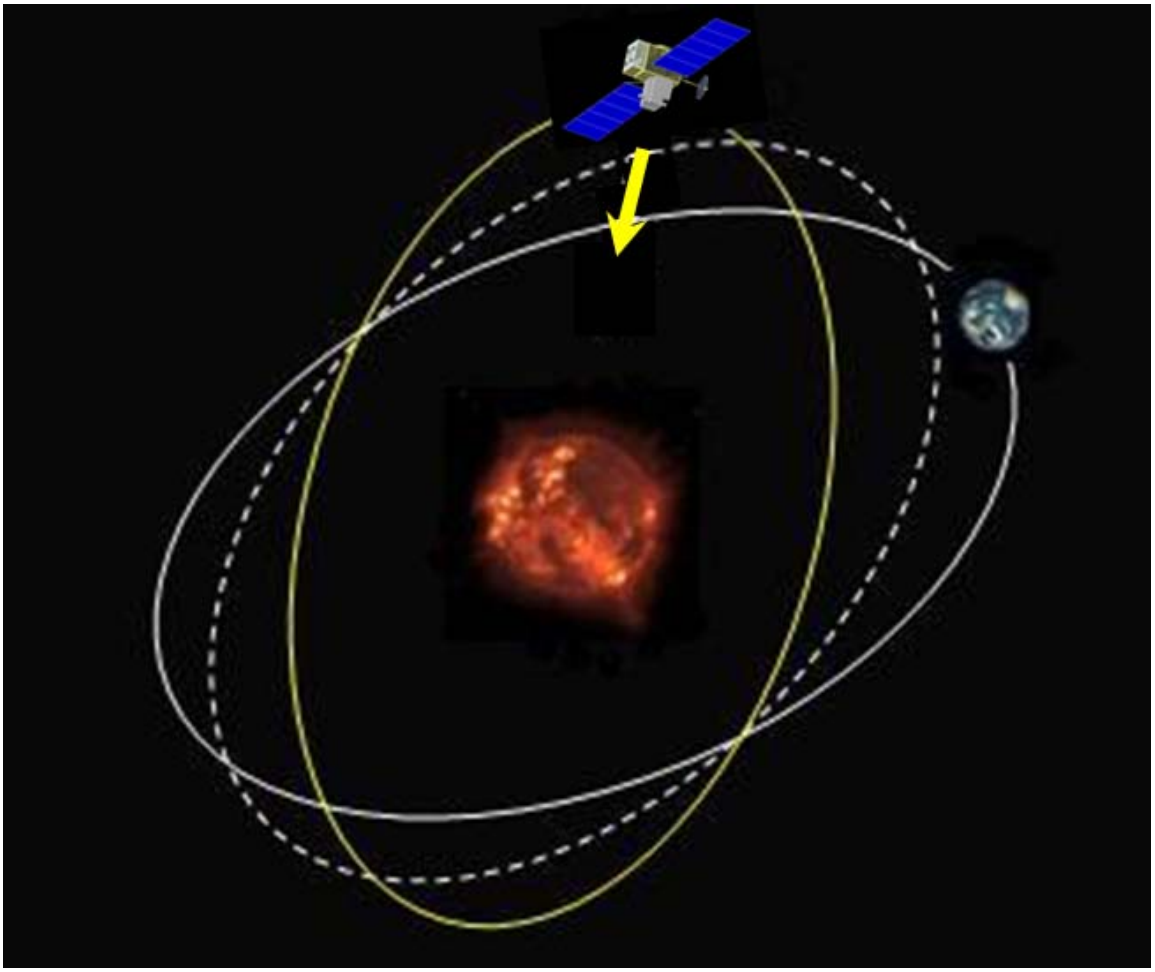

ISAS/JAXA SOLAR-C Working Group

Contents

Executive Summary

Scientific Background

Understanding the origins of solar magnetic activity has been at the forefront of solar and stellar physics since the discovery of the 11-year sunspot cycle nearly two centuries ago. Unraveling this mystery has broad implications not only for promoting a deeper knowledge of the Sun itself but also for understanding the Sun's influences on the heliosphere, the geospace environment, and potentially the Earth's climate system. Such influences regulate space weather, with increasing economic impacts on our technological society as our reliance on telecommunications systems, power grids, and airline travel continues to grow. As a readily observable example of an astrophysical magneto-hydrodynamic (MHD) dynamo, the Sun also provides unique insights into the generation of magnetic fields by turbulent plasma flows throughout the universe, from planetary and stellar interiors to stellar and galactic accretion disks to interstellar clouds.

The global magnetic polarity of the Sun reverses during each 11-year sunspot cycle so that the overall period of the solar magnetic activity cycle is 22 years. It is a formidable challenge to understand how such remarkable regularity arises from the highly turbulent conditions of the solar convection zone and how magnetic flux emerges from the solar interior to energize the solar atmosphere and power solar variability. Large-scale flows (differential rotation and meridional circulations) established by turbulent convection, plasma instabilities, and nonlinear feedbacks all play an important role, spanning many orders of magnitude in spatial and temporal scales.

Modern solar observations coupled with sophisticated theoretical and numerical models have yielded important insights into many aspects of solar magnetism but the basic physical mechanisms responsible for generating these fields are still not understood. To make great scientific progress in our understanding the Sun and the fundamental problems of cosmic magnetism, there is no doubt that we need to continue both theoretical and observational efforts. On the observational side, measuring solar internal flows is of the greatest importance. For this task helioseismology has proven to be a powerful tool.

Helioseismic measurements are based on surface wavefield data, normally and preferably temporal series of photospheric Dopplergrams, which are then analyzed to probe the solar interior structure and flows. With the so-called global methods, the wavefield data are used to measure (mainly acoustic) eigenfrequencies of the Sun. The eigenfrequencies are then analyzed, often by way of inverse methods, to probe the solar interior for thermal and dynamical structure of high degrees of symmetry, such as the spherically symmetric distribution of sound speed, or differential rotation as the axisymmetric component of flows. With new local methods, wavefield data are used to measure local resonant properties or wave propagation time for a given pair of points, by cross-correlating local wavefields. These travel-time data are then analyzed to probe the interior for local and/or asymmetric structures, such as meridional flow, convection and flows around active regions.

Differential rotation and meridional flows have already been measured by such helioseismology techniques, up to about 60° latitude with a typical uncertainty of the order of a m/s. It is essential to extend this measurement to the polar region, partly because without such measurement we will never be confident of our understanding of dynamics of the Sun as a whole, and partly because the polar region is where the magnetic flux reverses and the meridional flow, which plays an important

role in carrying the magnetic flux, should turn in towards the solar interior, and where polarity reversals take place in the surface layers.

Another related mystery is the total solar irradiance variation over the solar cycle. The total irradiance of the other solar-like stars that exhibits activity at a level that is similar to the Sun, on average varies around 0.3 per cent over their activity cycles. On the other hand, the solar irradiance varies only by 0.1 per cent. There is a well-founded suspicion that the solar irradiance depends on latitude, thereby creating a great interest in measuring the solar irradiance from high heliographic latitudes.

Science Objectives

SOLAR-C Plan A, from its highly inclined orbit around the Sun, aims to combine helioseismic and magnetic observations, solar irradiance measurements at various latitudes, and finally EUV and X-ray observations of the solar polar regions, to advance our understanding of solar variability.

The highest science objective of SOLAR-C Plan A is measuring subsurface flow at high-latitude regions, by local helioseismology techniques, based on Dopplergrams acquired by an HMI-MDI type instrument. From this measurement we will derive differential rotation, meridional circulations and convective flows in the upper convection zone. These flow-field measurements will then be cross-correlated with surface magnetic field measurement, to reveal how magnetic flux is transported to the polar region, and how the polarity reversals take place as interplay between plasma flows and magnetic fields. The predominantly vertical kG-field patches that *Hinode* has found in the polar regions are large enough to be observed. A serious attempt will also be made for stereohelioseismology, for investigating deeper layers, including the best ever shot of the solar tachocline region.

Solar irradiance measurements at various latitudes will, for the first time, enable us to measure the anisotropy of the total solar irradiance. The unexplained low photometric variability of the sun may be explained by higher variability at higher latitudes, likely caused by faculae. If it is not the case, then we must conclude that the Sun is a rather atypical star, which will lead to more fundamental questions in astrophysics.

The solar polar region also hosts various activity phenomena, and EUV and X-ray observations will be important in studying them, in particular atmospheric plasma flows in solar-wind source regions. Other scientific topics that SOLAR-C Plan A may address, exploiting its unique vantage point, include evolution of heliospheric structures (by a heliospheric imager) and cosmic-ray transport in the inner heliosphere (by a particle counter) when the optional payload is adopted..

Scientific Strategy

The outstanding issues confronting our current understanding of the solar dynamo may be summarized through several key scientific questions:

Q1) How is the global, cyclic, solar magnetic field generated?
Q2) What is the nature of flows in the polar regions of the Sun and how do they interact with magnetism?

Q3) How does the radiative energy output of the Sun depend on latitude?
Q4) How does magnetic activity shape the structure and evolution of the polar solar corona and how does it affect the Earth?

Progress on these scientific questions requires detailed observations of the solar polar regions, where data is currently scarce and where much of the subtle interplay between plasma flows and magnetic fields that gives rise to cyclic polarity reversals is thought to occur. The out-of-ecliptic observations of the Sun, for the first time, will provide an opportunity for detailed investigations of the magnetic structure and dynamics of the polar regions. High-latitude photospheric observations will also provide an unprecedented vantage point for helioseismic imaging that can be used to probe flows and fields in the deep convection zone and tachocline where solar activity is ultimately thought to originate.

In addition to measurements at the photospheric level, the structures of the outer solar atmosphere in polar regions and the heliospheric structures merit observations from outside the ecliptic. The poles of sun undergo dramatic change during the 11-year solar cycle, driven by the dynamo action in the solar convection zone. The polar vantage point gives unique opportunities for understanding the origin of the fast solar wind spectroscopically and for stereo viewing of surface vector magnetic fields, coronal structures, and Earth-directed CMEs in coordination with observatories near the Earth. The unique inclination for the SOLAR-C Plan-A observatory will also permit unprecedented measurements of the total solar irradiance. This may help resolve the discrepancy of the cycle variation of the solar irradiance of ~0.1% while solar analogs vary, on average, by 0.3%.

With this in mind, we propose the following prime measurement targets for the SOLAR-C Plan-A mission:

T1) Photospheric magnetic flux distribution and evolution in the polar regions
T2) Dynamical coupling between magnetic fields and flows
T3) High-precision measurement of total solar irradiance
T4) Structure and dynamics of the high-latitude solar corona and solar wind

The methodology, significance and expected scientific impact of each of these observational targets are discussed in Section 2.1.

Measurement Requirements

The following observables are required to address the SOLAR-C Plan-A top science objectives: (A) full-Sun photospheric line-of-sight Dopplergrams for measuring the subsurface flows by helioseismology, and (B) full-Sun photospheric magnetograms for tracking the evolution of magnetic fields on the surface.

These measurements must come from an orbit inclined to the solar ecliptic, with maximum orbit inclination ≥40°. The orbit must allow observations from >30°inclination for periods of >40 days for each polar passage. To maximize the telemetry available, the orbit shall be circular with a 1-year period, to synchronize the orbital motion of the spacecraft with that of the Earth.

The orbit gives a unique vantage point for the other science objectives. The following observables shall be taken to address them: (C) total solar irradiance, (D) full-Sun chromospheric images, (E) full-Sun transition region (TR) images, (F) full-Sun coronal images to monitor the dynamic activity and the evolution of high-latitude structures, and (G) emission-line imaging spectra in chromospheric, TR, and coronal lines for investigating the source region of fast solar wind and dynamics of the outer solar atmosphere, (H) visible-light images monitoring interplanetary space between the Sun and Earth, and (I) in-situ measurements including magnetic field, solar wind protons and electrons (TBD). Currently, (H) and (I) are treated as options in this Interim Report.

Photospheric magnetograms and Dopplergrams are made from multiple images. Not all the images can be transferred to the ground due to the expected telemetry rate, so onboard data processing and compression are mandatory to reduce the total data volume transferred, as was done on SOHO/MDI. The field of view for imaging observations needs to cover the full Sun with sufficient spatial sampling for each observable. The science requirements for image size, cadence and duration for the helioseismic observables are discussed in detail in Section 2.1. Table 3 shows estimates of the required data rates. A total average data rate of ~100 kbps is required.

SOLAR-C Plan-A Payload

The SOLAR-C Plan-A has been planned by attaching weight to science topics that are studied by remote-sensing instruments. The best condition for remote-sensing observations from the out-of-ecliptic orbit is selected under the restriction of current or near-future technology.

The science payload to satisfy the primary measurement requirements consists of:
- A visible light imager that can measure the full-Sun photospheric magnetic fields and line-of-sight Doppler velocity, similar to MDI on SOHO or a simplified version of HMI on SDO.
- A total irradiance monitor that measures the irradiance of the Sun. Multiple cavity monitors are needed for self calibration.
- A light-weight EUV imager that monitors the transition-region and coronal activity in the polar region.
- An EUV scanning spectrometer that measures the flow structures in the polar region.

The following instruments provide additional measurements of T4 and are listed as optional:
- A heliospheric imager that observes the space between the Sun and Earth
- In-situ instruments such as instruments measuring the solar wind and cosmic-ray particle sampler (TBD)

Trajectory and Orbit

The major mission requirement of SOLAR-C Plan A is to observe the Sun from high latitude, with target specified as 40°. In order to achieve this target, the SOLAR-C Plan-A Working Group has studied a number of possible mission designs using various trajectory manipulation techniques. The items considered are the tilt of the solar equatorial plane to the ecliptic, launcher capacity, planetary gravity assists, and the use of a highly efficient propulsion system. The launcher assumed is the Japanese H-IIA launch vehicle equipped with a solid motor upper stage. There are two possible options: one is to use solar electric propulsion assisted by an Earth swing-by (SEP option), and the

other is to use both Jupiter and Earth swing-bys (Jupiter option). The latter is a purely ballistic trajectory. The final orbit is nearly the same, a circular orbit with 1 AU distance from the Sun and 1 year orbital period, with a different time to reach the maximum inclination (5 years for SEP option and 7 years for Jupiter option). If there is a strong requirement that the spacecraft has to be in the final orbit before the solar maximum around 2024 (assuming launch in 2019), the SEP option is the only currently available way to satisfy the time constraint. The orbit profile in the cruise phase is quite different between SEP and Jupiter options. In the first three years, no observations are expected for the SEP option and there may be a short observing period of about a month at each hemisphere in the following years until the spacecraft enters into the final orbit. On the other hand, observations are possible at any time outside the swing-by operation for Jupiter option, but high telemetry is limited to positions near the Earth until reaching the final orbit.

Spacecraft

The SEP option requires a heavy propulsion system. The assumed μ20 ion engine system is an upgraded version of μ10 that was used in JAXA HAYABUSA sample return mission. The new engine itself has undergone endurance testing in the lab but no flight heritage yet. The μ20 ion engine system consumes 6 kW power, and a lightweight solar array paddle with large area is necessary. The total wet weight of the spacecraft in the SEP option is ~1,200 kg with payload mass of 130 kg. The total wet weight of spacecraft in the Jupiter option is ~750 kg with payload mass of 130 kg.

Launch vehicle

A single spacecraft launch with the JAXA H-II A rocket 202A is assumed. Some orbit cruise methodologies require a kick motor and it becomes one of new development items in the Japanese space agency after the interplanetary missions launched by M-III or M-V solid boosters. The use of a kick motor is assumed for both SEP and Jupiter options. There is a solution in a SEP option by an orbit cruise via Venus swing-by without having a kick motor by reducing the launch opportunity.

The spacecraft attitude is three-axis stabilized to meet the requirements of the imaging instruments. Angular momentum management occurs daily to weekly, using chemical thrusters. 300 kbps X-band downlink telemetry rate and 8 hr downlink time per day are assumed for an average data rate of 100 kbps, at a spacecraft distance at 0.56 AU from the Earth. Downlink stations are needed in the northern and southern hemispheres on Earth. 1 Mbps Ka-band telemetry rate at the same distance is under consideration to enable a greater telemetry volume.

1. SOLAR-C Mission Science Goals

1.1 Origin of Solar Magnetism

1.1.1 Solar Magnetic Cycle

The solar magnetic cycle is one of the greatest puzzles in astrophysics. Similar magnetic cycles have been observed in other stars; and the turbulent dynamo that controls these cycles is a key to understanding the cosmic magnetism. It has been known for centuries that the number of sunspots changes quasi-periodically with 11-year cycle, forming the famous "butterfly" diagram (Figure 1 and Figure 2).

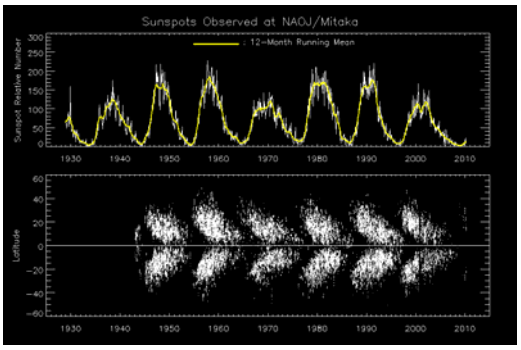

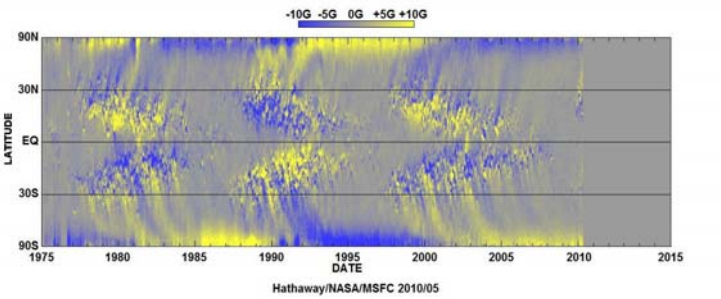

Figure 1: (left): Sunspot numbers and sunspot butterfly diagram (NAOJ)
Figure 2: (right): Averaged surface magnetic field strength (courtesy of D. H. Hathaway)

Many recent solar dynamo models are based on the so-called "flux-transport" paradigm whereby the advection of magnetic flux by the axisymmetric flow in the meridional plane regulates the period and amplitude of the activity cycle. Most flux-transport models attribute the generation of mean poloidal field to the emergence and subsequent dispersal of photospheric active regions by the combination of poleward circulation and turbulent diffusion in the upper convection zone, known as the "Babcock-Leighton" mechanism. The reversal of the global poloidal field occurs as opposite-signed field from lower latitudes converges on the polar regions. However, how this process couples to the dynamics and magnetic topology of the deeper convection zone is currently unknown. Recent *Hinode* observations reveal the polar field is highly structured, with magnetic field concentrations reaching 1kG, which is not captured by mean-field models. How the polar "magnetic landscape" changes with the solar cycle is one of the most critical questions for understanding the nature of solar magnetism. The magnetic field evolution is intimately coupled to the flow field, including convection, differential rotation, and the mean meridional flow. In particular, the latitudinal bands of photospheric magnetic activity reflected in the solar butterfly diagram (Figure 1 and Figure 2) are closely linked to systematic variations in the differential rotation known as "torsional oscillations" (Figure 3). A surprising result from helioseismology is that the depth and strength of these flows increase in the near-polar regions. Furthermore, models of surface flux transport indicate that the polar field strength is sensitive to variations in the amplitude and structure of the high-latitude meridional flow. However, reliable measurements of the magnetic and flow fields in the near-polar regions are currently lacking.

There is a huge gap in our knowledge of the polar magnetism and dynamics, preventing us from understanding the basic mechanisms of solar magnetic activity, and developing physics-based forecasts of the solar activity and cycles.

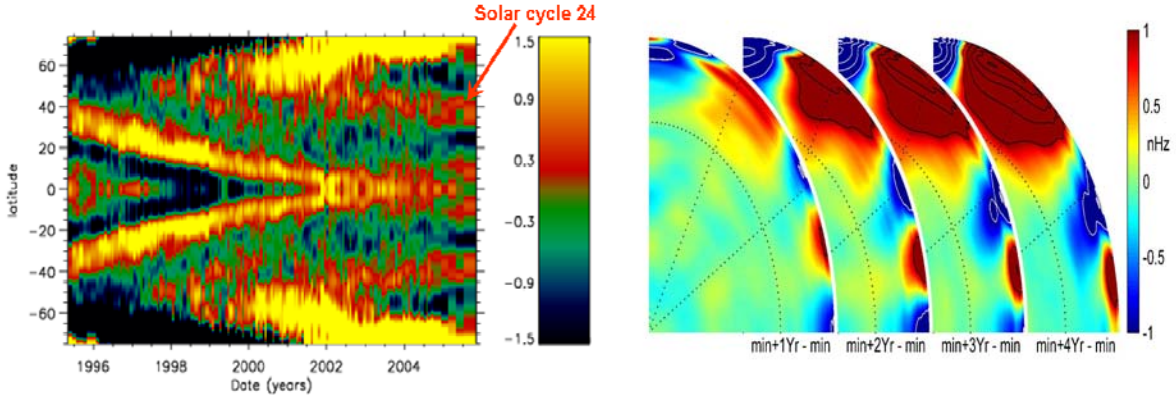

Figure 3: Systematic variations in angular velocity known as torsional oscillations, illustrating their latitudinal and temporal variation several Mm below the photosphere (left) and their subsurface structure in the meridional plane (right; figure adapted from Vorontsov et al. 2002).

1.1.2 Generation and Emergence of Magnetic Field

In astrophysical objects, dynamo action can exist in plasmas with a seed magnetic field and flow fields. However, sufficient conditions for dynamos are not well-determined. For solar and stellar physics it is particularly important that dynamo processes can result in a cyclic behavior. Mean-field MHD theories of solar and stellar dynamos predict the cyclic behavior, which resembles the observed properties such as the butterfly diagram for sunspot formation zone and polar field polarity reversals. However, our understanding of the underlying physical processes is still schematic Parker's standard α-Ω mechanism that has been applied to the Sun and a wide range of other astrophysical objects, stars, galaxies, interstellar medium.

The current global dynamo models involve several building blocks mainly known by their representation in mean-field electrodynamics: One is the α-effect that generates the poloidal field from the mean poloidal or toroidal field by a turbulent cyclonic flows (Item 1 in Figure 4), or by a disintegration of the surface active region fields. (Items 1', 4, and 5 in Figure 4). The other is the Ω-effect that generates the toroidal field from the mean poloidal field by shear motions in the differential rotation. These two effects couple with each other to re-generate the toroidal and poloidal fields in repetition. The locations of each effect are now considered to be separated in the interior, so that , in addition to these field stretching mechanisms, the transport of the fields are also important ingredients: (Items 3 and 3' in Figure 4). The three different transport mechanisms generally considered are active transport toward the surface by means of magnetic buoyancy (rising flux tubes, formation of active regions), turbulent transport in the convection zone (turbulent pumping, turbulent diffusion) and transport by the large scale meridional flow (flux transport dynamo; Figure 5).

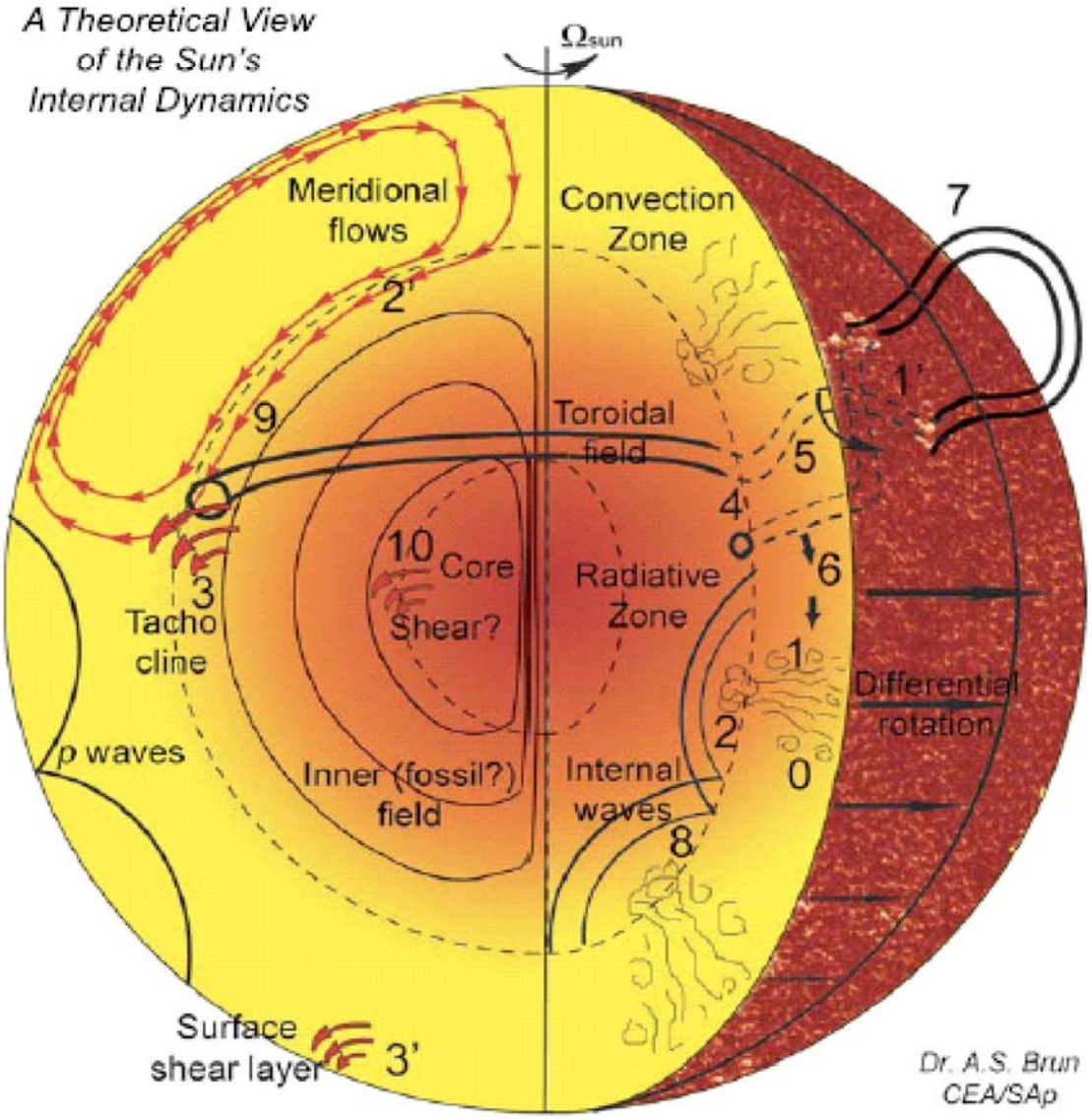

0: Turbulent convection (plumes); 1: Generation/self-induction of poloidal B field ("α-effect") or 1': Tilt of active region; 2: Turbulent pumping of B field in tachocline or transport of B field by meridional flows from CZ into tachocline (single for multi-cells flow?); 3: Field ordering into toroidal structures by large-scale radial and latitudinal shear in tachocline ("Ω-effect"); 3': Surface shear layer or subsurface weather; 4: Toroidal field becomes unstable to m=1 or 2 longitudinal instability (Parker instability); 5:Rise and rotation of twisted toroidal structures; 6: Recycling of weak field in CZ; 7: Emergence of bipolar structures at the surface; 8: Internal waves propagating in RZ and possibly extracting angular momentum; 9: Interaction between dynamo induced field and inner field in the tachocline along with shear, turbulence, waves, etc.; 10: Instability of inner field and shearing via Ω-effect at nuclear core edge? Is there a dynamo loop realized in RZ?

Figure 4: Solar internal dynamics and dynamo

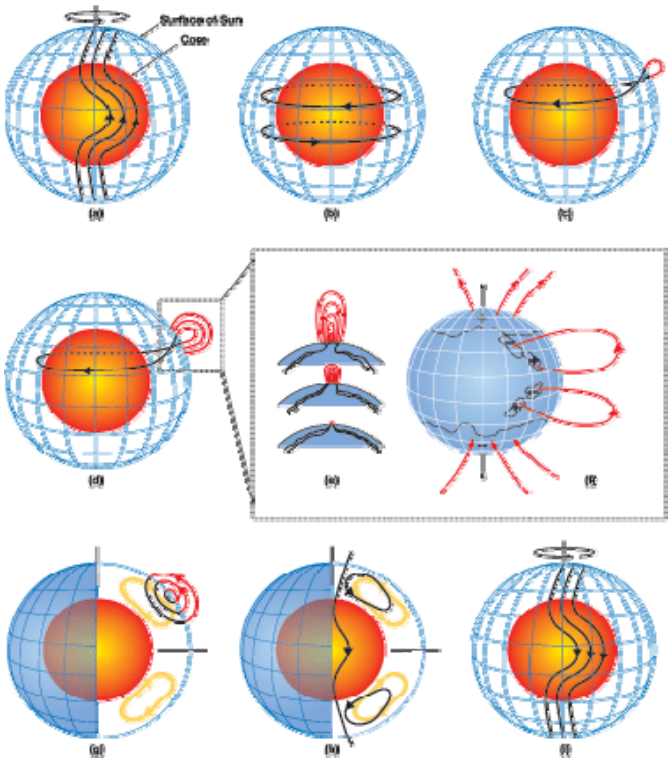

Figure 5: Flux transport dynamo (adapted from Dikpati and Gilman 2006)

The success of this beautiful theory hinges on the turbulent properties, magnetic and kinetic helicities and diffusivity. However, direct numerical simulations, developed during the past decade, revealed significant limitations, such as the catastrophic helicity quenching, which severely restricts the magnetic field growth. The potential solution is in studying the helicity balance including large-scale circulations and helicity loss through coronal mass ejections. This study requires detailed observations of the solar interior, magnetic field and coronal dynamics over the whole solar cycle. It is particularly important to understand the mechanism of the cyclic polar field reversals revealed in synoptic ground-based observations during the past three sunspot cycles. Because the Sun's axis is almost perpendicular to the ecliptic our knowledge of the polar magnetic field structure and dynamics is very poor.

The best opportunity to gain this knowledge can be provided by the out-of-ecliptic SOLAR-C mission. It will provide an important insight into the structure of polar magnetic fields and the mechanism of polarity reversals. The polar fields are largely unipolar, and it was believed that the polarity reversals result from a diffusion or circulation process of magnetic flux transport from the low-latitude zone where the flux emerges. However, recent high-resolution observations from *Hinode* showed that the polar fields are highly structured, and, while the mean polar field is only a few Gauss, the field in these elements is very strong. This discovery challenges the flux transport models, and opens a new opportunity of studying the relationships between the structuring and global field reversals. The out-of-ecliptic mission will also improve our knowledge of the large-scale convection, differential rotation and meridional circulation, which are the key ingredients of dynamo models.

In terms of magnetic-field observations, compared to ultra high-resolution vector-magnetograms obtained in the ecliptic plane, SOLAR-C has advantages in longer observation periods, more global view of the polar regions, and capability of providing simultaneous flow-field observation in and below the photosphere, to facilitate study of interaction between plasma flow and magnetic fields. Potential disadvantages are that part of the polar regions that lie on the Earth-side may be observed with higher resolution from the ecliptic plane, and the lack of vector magnetogram capability from the spectro-polarimetry by an imaging polarimeter. If, however, as *Hinode* is finding out, the polar fields primarily comprise relatively large, predominantly vertical kG-field patches, these disadvantages may not be so important.

1.1.3 Dynamics of the Solar Convection Zone and Tachocline

The differential rotation, meridional circulation, turbulent α-effect, and turbulent transport terms (turbulent diffusion and magnetic pumping) that form the basis of the solar dynamo models ultimately arise from turbulent solar convection. Stellar observations confirm that convection breeds magnetism; late-type stars such as the Sun with convective outer envelopes exhibit vibrant magnetic activity whereas more massive stars with convectively stable envelopes are generally less active. Thus, understanding solar convection and the mean flows it generates is an essential prerequisite to understanding solar magnetism.

Determination of the solar internal rotation profile and near-surface meridional circulation by means of global and local helioseismology, in the past three decades, has revolutionized solar dynamo theory. Rotational shear has long been an essential ingredient in all solar dynamo models, as the principle generation mechanism for the global-scale toroidal magnetic flux (Ω-effect) that ultimately emerges from the solar interior to form active regions. More recent flux-transport dynamo models have further identified flux advection by the mean meridional circulation as a key factor in the establishment of cyclic magnetic activity. In particular, the poleward advection of emergent toroidal flux from lower latitudes may account for the polarity reversals of the polar field and thus the cyclic reversals of the global dipole moment. Possible correlations between the high-latitude meridional flow speed and activity patterns such as cycle amplitude and duration are necessary to distinguish among various dynamo paradigms. Regardless of the dynamo mechanism, surface flux transport models indicate that the strength and distribution of the polar magnetic field (crucial for coupling to the heliosphere) is sensitive to the amplitude and structure of the high-latitude meridional circulation. Determination of the differential rotation and the meridional circulation in the polar regions will thus provide unprecedented insights into the dynamics of the convection zone, the operation of the solar dynamo, and the solar-terrestrial interaction, bringing the helioseismology revolution to its ultimate fruition.

Observations of the solar photosphere reveal a hierarchy of convective motions, from solar granulation (L~1 Mm) to supergranulation (L~35 Mm). Deeper in the convection zone convective length and time scales increase as a consequence of the larger density and pressure scale heights.

Magnetic flux transport by supergranulation and granulation may contribute to the cyclic reversal of the large-scale poloidal field by working in concert with the meridional circulation. Not only does convection influence magnetism, but the converse is also true; magnetism can influence the structure of convection and investigating the nature of this nonlinear feedback provides valuable insight into both phenomena. In particular, the structure and evolution of supergranulation in polar coronal holes, where a net unipolar flux permeates the photosphere, may be significantly different

than that at lower latitudes where the flux distribution exhibits mixed polarity. The Lorentz force tends to decrease convective length scales but magnetically-induced enhancements in radiative cooling may counteract this effect. Careful observations over extended time intervals (at least hundreds of days for reliable statistics) at high latitudes are needed to elucidate the subtle nonlinear feedbacks between solar convection, magnetism, and radiation.

Observational signatures of giant cells are notoriously difficult to glean from photospheric observations but the unique high-latitude vantage point offered by SOLAR-C will provide new opportunities. The maintenance of mean flows by global convective motions is expected to produce thermal gradients between the equator and pole that may be detectable by helioseismic inversions or photospheric irradiance measurements (Section 1.2.3). Furthermore, theoretical and numerical models predict a change in morphology between global convective motions at high and low latitudes in rotating spherical shells. The transition between polar and equatorial convective modes occurs near the so-called tangent cylinder, a cylindrical surface aligned with the rotation axis and tangent to the base of the convection zone. This tangent cylinder intersects with the solar surface at about 45° latitude. Possible changes in the subsurface flow fields inferred from local helioseismic inversions inside and outside the tangent cylinder may provide a valuable and previously unexploited observational signature of the elusive but extremely important giant cells. *Hinode* measurements have already revealed a systematic high-latitude alignment of supergranules that may reflect the underlying influence of giant cells. Polar observations may also reveal other phemonema such as inertial waves or precessing convective modes with longitudinal wavenumber m=1, as seen in some numerical simulations.

Convective and meridional flows that converge toward the poles are accelerated in a prograde sense by means of the Coriolis force which can in some circumstances establish a cyclonic polar vortex. The presence of a polar vortex remains controversial in current helioseismic inversions but is exhibited by some numerical simulations. Coordinated helioseismic determinations of the differential rotation and meridional flow at high latitudes will settle this issue, at least in the upper convection zone, and will provide important constraints to global convection simulations, enhancing our understanding of angular momentum transport.

Like the polar regions, the base of the solar convection zone is an unexplored frontier of essential importance to the operation of the solar dynamo. This is where photospheric active regions originate, as the strong shear, convective pumping, and mild stratification promote the generation of coherent toroidal magnetic flux structures which buoyantly destabilize and rise. Flux-transport dynamo models attribute the duration of the solar cycle to the equatorward flow speed near the base of the convection zone. Furthermore, recent theoretical and numerical models indicate that the differential rotation profile throughout the solar convection zone is influenced by thermal and mechanical coupling to the tachocline. SOLAR-C will enable fundamental breakthroughs in our understanding of solar internal dynamics and magnetism by probing the base of the convection zone through the innovative and powerful technique of stereoscopic helioseismology (Section 1.1.4).

1.1.4 Probing the Solar Interior

In our effort to understand the mechanism behind the solar activity cycle, it is important that we study the solar interior observationally. The only method known to us is helioseismology, which

enables us to measure thermal structure and flows in the solar interior. In this subsection a very brief introduction to helioseismology is given, to provide background for further discussions in Section 2.

The solar 5-minute oscillations, discovered by Leighton et al (1962), were later identified as manifestation of the global acoustic eigenoscillations, excited by acoustic emission by turbulent convective motions. These eigenmodes are results of acoustic waves generated in the upper convection zone travelling around the sun, some of which interfere with themselves constructively and become resonant modes, whose properties are sensitive to the structure of the sun (Figure 6). This motivated effort to develop methods of probing the solar interior based on precisely measured eigenfrequencies.

In helioseismology, we start from observing surface wavefield, preferably by Doppler velocity measurement, which is known to suffer less noise compared to intensity fluctuation measurement (by a factor of 5 or more is not uncommon). The wavefield is then characterized by Fourier (in temporal domain)/Spherical Harmonic (in spatial domain) analyses, to produce eigenfrequencies as the primary product. The eigenfrequencies are then analyzed, typically by inversion methods, to estimate various quantities that affect wave propagation. One good example is adiabatic sound-speed distribution, and another is differential rotation in the sun (Figure 7), which is now measured in low- to mid-latitude convection zone and deeper into the radiative zone, but not at high-latitudes and in the central region of the sun. The limitations are mainly coming from an insufficient number of eigenmodes that sample these regions. The profile of the solar differential rotation depicted in Figure 7 gave observational constraints to solar dynamo theory. In fact, it contradicted columnar rotation profiles which were generally believed to be the case for the sun, and understanding of dynamo were based on.

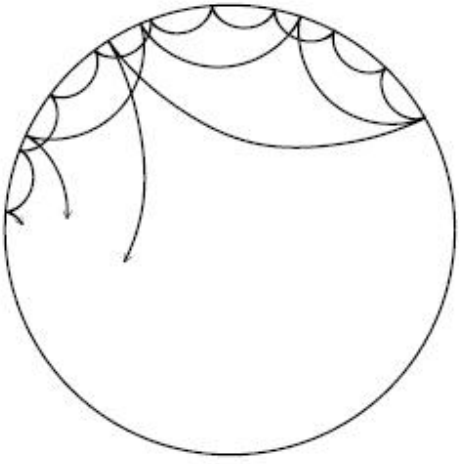

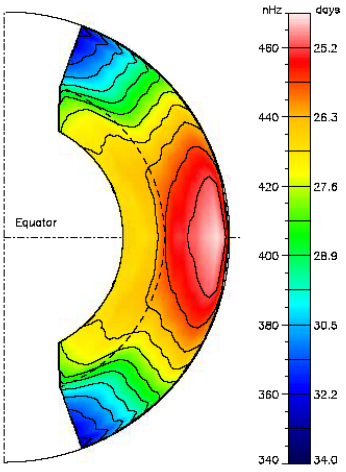

Figure 6. (left): Acoustic ray paths for various modes. Each of these paths, after a trip around the sun, eventually overlap with itself, and if it is found to be constructively interfering with itself, it becomes a resonant eigenmode. Different modes have different paths, and therefore sample different parts of the sun.
Figure 7. (right): Differential rotation of the sun measured by (global) helioseismology (adapted from Thompson et al 1996).

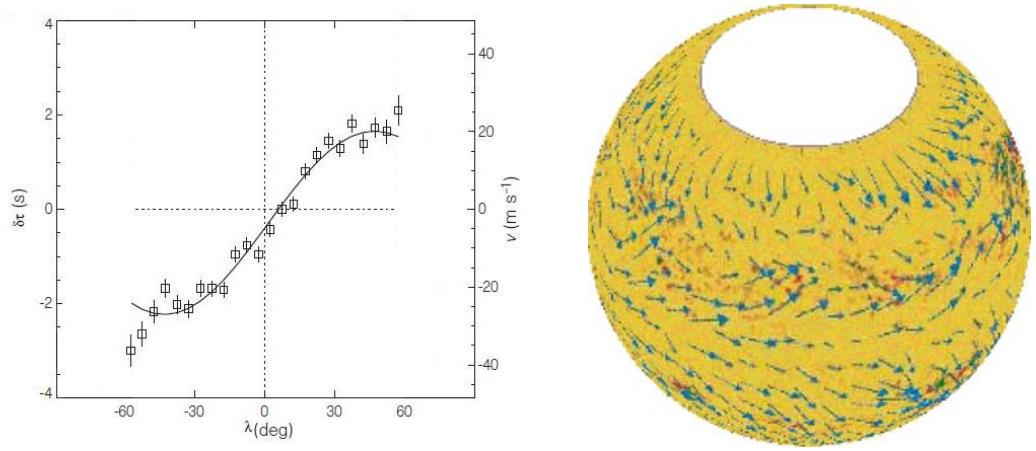

Figure 8. (left): Meridional flow speed measured by local helioseismology (adapted from Giles et al 1997) Figure 9. (right): Subsurface local flows measured by a local helioseismology technique (adapted from Haber et al 2002).

Building on these successes, in recent years, a new subfield of *local* helioseismology is developing. As in the old version of helioseismology (often called *global* helioseismology), local helioseismology does start from measuring wavefields. In local helioseismology, however, we do not measure (global) eigenfrequencies. Instead, we measure those quantities that characterize *local* propagation of the waves, such as wave travel times between a pair of surface points (for example, two bouncing points along a ray path in Figure 6), power distribution (in wavenumber-frequency space) of local wavefield, etc. Unlike in global helioseismology, these measurements provide bases for probing *localized* and *asymmetric* structure of the sun, not constrained by the symmetric manner in which global modes sample the sun, as signified by symmetries of eigenfunctions.

Meridional circulation has thus been measured (Figure 8) by a time-distance method, and solar subsurface 'weather' patterns (local flowfields) are now routinely measured by local power spectrum analyses (Figure 9). Once again, the high-latitude regions are missing as, once beyond about 60° off the disc centre, foreshortening and projection degrade the local wavefield measurement significantly, although these parts are of great interest. Deeper layers are also difficult to access, because of the following. As we see in Figure 6, probing a deeper layer requires measuring wavefields at (at least) two regions on the sun that are apart by a great distance, in which case at least one, possibly both, of the region tends to be rather close to the limb, and therefore suffers from projection and foreshortening. One possible way to resolve this difficulty is *stereohelioseismology*, in which multiple helioseismic observations from different view angles are used to observe wavefields without significant degradation due to projection and foreshortening.

1.1.5 Prediction of Solar Cycles

Prediction of the solar sunspot cycles is not only of great practical importance, it also represents an ultimate test for our understanding of solar magnetism. So far, our predictions based on the α-Ω dynamo were not successful even with the input from helioseismology. The most successful prediction of the previous solar cycle was made using measurements of polar magnetic field of the Sun (Figure 10). The polar magnetic field reaches the maximum strength during the sunspot minima, and it correlates very well with the maximum sunspot number of the following solar cycle. In addition, it has been established long ago that a close correlation exists between the strength of

geomagnetic indexes measured during the solar minima with the following sunspot maxima. This correlation is probably caused by the high-speed solar wind from the polar regions.

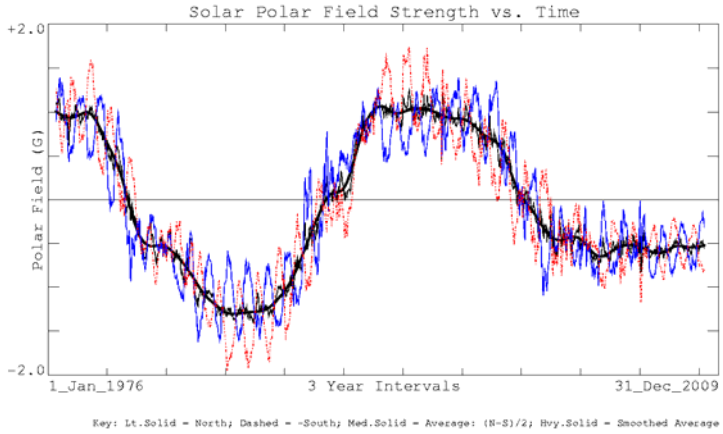

Figure 10. Evolution of solar polar magnetic fields (solid: north and dashed: -south)

However, how the polar magnetic field strength is translated into the future sunspot number is completely unknown. It has been suggested that this may correspond to the transformation of the global dipole magnetic field into the toroidal magnetic field of sunspots by the differential rotation (Ω-mechanism of the dynamo). However, the physics of this transformation and also the mechanism, which determines the polar magnetic field strength, are unknown.

Thus, for developing physics-based forecast of solar activity it is extremely important to investigate the structure and evolution of the polar magnetic fields, mechanisms of the magnetic flux transport and interaction between the old and new magnetic fluxes. The SOLAR-C observations will provide direct measurements of magnetic fields and flows, which will be incorporated into the dynamo models and data assimilation procedures for predicting the solar magnetic cycles. In addition, it is well-known that the solar 11-year cycles have a complicated structure with periods of very high activity. It will be very important to investigate the correlation between these periods and the preceding polar dynamics.

1.1.6 Scientific Questions to be Solved by SOLAR-C

We set the following four fundamental questions toward the understanding the solar magnetism and 11-year activity cycle related issues that are tackled by SOLAR-C.

Q1) How is the global, cyclic, solar magnetic field generated?
Q2) What is the nature of flows in the polar regions of the Sun and how do they interact with magnetism?
Q3) How does the radiative energy output of the Sun depend on latitude?
Q4) How does magnetic activity shape the structure and evolution of the polar solar corona and how does it affect the Earth?

The relation between these questions and what targets should be observed with the science payload is shown in Table 1. The detailed description on the background is shown in the following sections.

Table 1: Summary of scientific questions, targets and the required observations.

Key Questions	Section	Observation Targets; overview	Observation Targets in detail	Instruments / Measurements	Scientific objectives/Background in brief	Importance / Difficulty
Q1: How is the global cyclic, solar magnetic field generated ?	1.2.1	T1) Dynamical coupling between magenetic fields and flows	* Surface meridional circulation beyond latitudes of 60 degrees * Surface magnetism * Polar magnetic field reversal * Cyclic variation of above variables	* Doppler for Local HS * Magnetic (longitudinal)	* Possible correlations between the hihg-latitude meridional flow speed and magnetic activity patterns are necessary to distinguish between different dynamo paradigms. * Determining the differential rotation profile close to the poles will provide	important / definite
Q2: What is the nature of flows in the polar regions of the Sun, and how they vary with magnetic field?	1.2.2	T2) Photospheric magnetic flux distribution and evolution in the polar regions	* Transport of magnetic flux by super-granular flows in the polar region * Differential rotaion in the polar regions	* Magnetic (vector) * Granular patterns	* Constrain the amplitude of turbulent flux dispersal from models that describe the surface evolution of magnetic field, that limit the processes rebuilding the poloidal field from troidal field. * Small versus large scale dynamo	moderate / definite
			* non-axisymmetric flows	* Doppler for Local HS	* Limit the efficiency of poloidal field generation	important / definite
			* Jet-like flow associated with the flux tubes in the tachocline * Flows associated with flux emergence	* Doppler for Global HS from additional vantage points	* Possible limitation for the field structure and amplitude in the solar convection zone	very important / very difficult
			* Near-surface super-granular-scale convection in the polar regions * Global convection, giant cell	* Doppler for Local HS * Magnetic (longitudinal)	* Progress into understanding convective transport and the establishment of mean flows in the deep convection zone.	important / difficult
			* Meridional counter flow * Thermal structure in the convection zone	* Doppler for Global HS from additional vantage points	* Unprecedented insights into the dynamics of the deep convection zone.	very important / very difficult
Q3: How does the radiative energy output of the Sun depends on latitude?	1.2.3	T3) High-precision measurement of total solar irradiance	* Continuous measurement of the total solar irradiance from various solar latitues	*Total irradiance	*Understand the irradiance variation against latitude *Understand the irradiance variation in stellar activity cycles	very important / definite
Q4: How does magnetic activity shape the structure and evolution of the polar solar corona and how does it affect the Earth ?	1.2.4	T4) Structure and dynamics of the high-latitude solar corona and solar wind	* Imaging and spectroscopy in EUV emission lines for outer solar atmosphere * White-light imaging of heliospheric structures between the Sun and Earth * In-situ measurements of the solar wind and particles (including cosmic rays)	*EUV Imager *EUV Imaging Spectrograph *Heliospheric Imager (optional) *In-situ instruments (optional; not clearly defined yet)	*Progress of understanding the variation of polar coronal structures in a solar cycle *Progress of understanding polar region dynamics in outer solar atmosphere *New view by direct imaging of innter heliosphere from a vantage point *Progress in understanding the	important/ definite

1.2 Exploration of Solar Interior and Solar Magnetic Activity

The primary goal of the SOLAR-C mission is to understand the origin of solar magnetic activity by observing the magnetism and dynamics of the polar regions that are currently inaccessible for direct observation. In Section 1.1 we identified four key scientific questions tackled by SOLAR-C. They are summarized in Table 1. Here we describe each of the observational targets in turn and what scientific impact they are likely to have.

1.2.1 Q1: How is the global, cyclic, solar magnetic field generated?

Understanding the origin, distribution, topology, and evolution of magnetic flux near the solar poles is essential for understanding the origins of cyclic magnetic activity, for predicting the amplitude and duration of future cycles, and for assessing the impact of solar variability on the Earth. Coupling between magnetic fields and flows in the polar regions governs the polarity reversal of the global dipole moment and shapes the magnetic topology of the overlying corona. The magnetic flux emanating from polar coronal holes fills the heliosphere and accelerates the fast component of the solar wind, thus regulating the interaction between the Sun and planetary space environment. Further progress requires high-latitude magnetograms, Dopplergrams, and helioseismic imaging.

Synoptic observations of solar magnetic fields have shown evidence that the magnetic flux at the following (westward) edge of bipolar active regions is systematically transported toward the poles, where it encounters poloidal flux of the opposite sign generated by the previous cycle. As low-latitude flux continues to accumulate, the magnetic polarity of the polar regions reverses, leading to a corresponding reversal in the global dipole moment. ***However, how the process of the polarity reversal actually occurs in detail and how it couples to the deeper convection zone is unknown.*** What processes determine the distribution of surface and subsurface polar flux before and after a reversal? This fundamental issue can and will be resolved by means of a magnetograph viewing the pole from an inclination much greater than the 7° provided by the ecliptic.

High-latitude magnetic field measurements are also needed to quantify the energy and flux budget of the dynamo, the multipolar structure of the mean poloidal field, and the efficiency of poloidal field generation by means of the Babcock-Leighton mechanism. Evidence for non-axisymmetric structure in large-scale fields with low longitudinal wavenumber (m=1-3) might reflect the presence of MHD shear instabilities. Measurements of the high-latitude magnetic field in the solar photosphere are of fundamental importance for the understanding of the magnetic topology of the solar corona and its dynamical coupling to the solar interior, particularly with regard to small-scale flux emergence and coronal heating.

A complete understanding of how a polar field reversal occurs and what physical processes give rise to the solar activity cycle can only be obtained by considering magnetic field measurements within the context of the global and local flows that generate them. This is addressed in question Q2, Section 1.2.2.

1.2.2 Q2: What is the nature of the flows in the polar regions of the Sun and how do they interact with magnetism?

As alluded to in Sections 1.1.2 the dynamical origins of solar magnetic activity can only be fully investigated by considering correlations between multiple observables. The most important correlations are clearly those between the flow and the magnetic fields. Magnetic induction by convection, differential rotation, and meridional circulation is responsible for the magnetic activity patterns we see and the back-reaction of the Lorentz force on mean and fluctuating flows provides an important diagnostic of subsurface dynamics. Investigating such interactions lies at the heart of nearly all of the scientific objectives of the SOLAR-C mission.

Differential rotation and meridional flow in polar regions

Details of differential rotation and meridional flow in polar regions are currently unknown. Differential rotation is inferred from global acoustic oscillations, which are not very sensitive to the structure in high latitudes and in addition they do not allow for a discrimination between contributions from the southern and northern hemisphere. Meridional flows are inferred from Doppler measurements as well as local helioseismic techniques. Both approaches yield only reliable data to latitudes of about 60° since resolution is limited due to foreshortening and, in the case of helioseismic measurements, the signal to noise ratio is reduced due to the line-of-sight projection of the p-mode Doppler signal.

Existing helioseismic measurements of differential rotation suggest sharp spatial and temporal variations, including the possibility of a subsurface poleward jet (polar jet), but these measurements can be confirmed only by observing the polar regions directly, from an out-of-ecliptic orbit and by local helioseismology, which is free from the constraints of global helioseismology. The zeroth-order structure of the meridional flow is approximately described by a single cell pattern with poleward flow near the surface (and maybe in equatorward at the bottom). An additional flow cell with opposite direction in polar regions has been inferred from some measurements, but is still strongly debated. In addition to their dynamo implications differential rotation and meridional flow have compelling diagnostic value in understanding the dynamics of the deep solar convection zone. Particularly significant are possible correlations between zonal flows, meridional flows, magnetic flux, and thermal variations.

The most well established signature of dynamical coupling between the zonal and meridional flows, magnetic fields, and thermal gradients is that of the solar torsional oscillations. These are alternating bands of east-west zonal flow that evolve in close correspondence with the solar activity cycle (Figure 3). Two components are evident from the data, including a low-latitude branch that propagates equatorward in conjunction with bands of magnetic activity and a high-latitude branch that propagates poleward on a comparable time scale. The high-latitude branch is stronger and deeper than the low-latitude branch and may arise from distinct dynamical influences. Correlated meridional flows and thermal signatures are known for the low-latitude branch but are currently undetectable for the high-latitude branch. Variations of the meridional flow with the solar cycle induced by magnetic or thermal forcing also have important consequences for determining the strength and distribution of the polar field and the timing of polarity reversals. Coordinated observations of the meridional flow and the magnetic field in the polar regions will provide quantitative estimates of flux transport and will thus elucidate the physical mechanisms that underlie cyclic solar activity.

The vantage point of SOLAR-C will provide an unprecedented opportunity to observe such correlations and in particular their phase relationships, providing important constraints to theoretical and numerical models of the solar convection zone and dynamo by exploring a part of the Sun that is virtually unknown.

Tachocline dynamics/stereoscopic measurements

In order to observationally constrain the subsurface location of dynamo activity it is necessary to detect either field-induced perturbations of the sound speed or related flow fields. Sunspots and related bipolar active regions in the solar photosphere are thought to originate from the buoyant destabilization and subsequent emergence of strong, coherent toroidal magnetic flux structures that are generated deep in the solar interior, most likely in the tachocline or the lower convection zone. Some theoretical and numerical models predict that such concentrated toroidal flux structures may support coincident zonal jets of fluid as large as 100 m/s that help stabilize them against magnetic tension and buoyancy. Although direct detection of such deep-seated toroidal magnetic flux structures may be beyond the sensitivity of helioseismic inversion techniques, the zonal jets they induce may be detectable by stereoscopic helioseismology in which coordinated observations using SOLAR-C and another instrument such as HMI or GONG would provide the very long baselines needed to measure the relatively long-wavelength modes that sample the deep interior with local helioseismology.

Currently one of the most pressing issues concerns the strength of the subsurface toroidal fields that ultimately emerge to produce photospheric active regions; current estimates range from 10 to 100 kG. The predicted amplitudes of associated zonal jets increase with the strength of the field, and are potentially only detectable toward the higher end of the estimated range (100 kG). Detections or even upper limits of this order for zonal flows and toroidal field strengths in the deep convection zone and tachocline could have a dramatic impact on dynamo models.

Stereoscopic helioseismology will also allow us to improve measurements of the meridional flow in the deep convection zone. Such measurements are challenging but extremely important, since the meridional flow speed at the base of the convection zone largely sets the 22-year period of the solar activity cycle, according to current flux-transport dynamo models. Given the paucity of current data, any limit imposed on structures, speed, etc. by observations would be of great importance. For example, determining the depth at which the flow shifts from poleward to equatorward would improve current estimates of the speed of the return flow at the base of the convection zone based on mass conservation. The density contrast of 100 between the lower (0.7R) and upper (0.96R) convection zone implies values of order several m/s, which would be extremely difficult to measure directly, even with a stereoscopic method.

In addition, the tachocline might also play a central role in determining the structure of differential rotation throughout the convection zone (deviation from Taylor-Proudman state, in which the rotation rate remains constant along the direction parallel to the rotation axis). Here additional constraints on the thermal structure, especially latitudinal temperature variations are crucial. Current attempts to measure such variations using the GONG and MDI data will be greatly improved by supplemental data from the unique perspective of SOLAR-C. The required accuracy is substantial, since models predict only a few Kelvin variation, as compared with a background temperature of about 2 million K at the base of the convection zone. Yet, if magnetic effects can be

properly taken into account, local helioseismic inversions and irradiance measurements (Sec. 1.2.3) may be able to provide some estimate of the pole-equator temperature difference in the solar surface layers, if not in the deep convection zone.

Stereoscopic techniques will also benefit global helioseismic inversions, which are currently impeded by incomplete sampling of the solar surface. Observations from a single vantage point only sample one side of the Sun rather than the entire spherical surface on which spherical harmonic functions would form an orthogonal set. Multiple vantage points would greatly improve spatial coverage. In case of SOLAR-C, with its position in the orbit around the Sun synchronous with Earth, for maximizing the telemetry rate, the increase in spatial coverage is not so great but it still offers an increase particularly when its heliographic latitude is high.

Determining the differential rotation, the meridional flow, and convective patterns in the upper convection zone at high latitudes will be achieved by applying well-established local helioseismology techniques previously confined to lower latitudes. Probing deeper layers will be done by a novel technique of stereoscopic helioseismology from multiple vantage points.

1.2.3 Q3: How does the radiative energy output of the Sun depend on latitude?

The main goal of the proposed SOLAR-C Luminosity and Irradiance Monitor (LIM) is to address the basic question, 'How precisely do we know the luminosity of the Sun?' A more detailed description of the science goals can be summarized by the following four fundamental questions related to the radiative output of the Sun:

• *Are the solar irradiance variations observed from Earth due to flux redistribution in space or due to solar luminosity variations?*
• *Is the radiant output at the poles different from the values we observe in the ecliptic?*
• *What is the latitudinal temperature gradient?*
• *Why is the variability in irradiance of the Sun a factor of three smaller than that of sun-like stars?*

The first three questions arise because up to now, the irradiance was observed exclusively from the in-ecliptic vantage point. The fourth question was first asked by Lockwood et al. (1992) who noted that compared with Sun-like stars, the irradiance variations induced by the solar cycle appear to be smaller than in Sun-like stars. It has been proposed that this exceptional property of the Sun is due to our equator-on viewing angle (Lockwood et al. 1997, Radick 1998) but it is not yet clear whether this explanation can fully account for the observed difference (Knaack et al. 2001).

The observational answers to these fundamental questions require measurements of the solar radiative output at higher heliospheric latitudes than what an ecliptic-bound mission can provide. Observations from the SOLAR-C Plan-A platform will allow us to verify the view-point hypothesis. SOLAR-C Plan-A is the only planned mission that intends to fly a radiometer out of the ecliptic. On average, stars are seen from a latitude of 30º. A trend in the solar irradiance level as SOLAR-C LIM approaches this inclination will allow us to confirm or reject the view-point hypothesis. This measurement will also be possible check the reliability of TSI models at the Maunder minimum era that were reproduced using various indices with basic data of cosmogenic isotope that record the past solar magnetic activity. This is of vital importance in the future TSI prediction for the Earth's environment.

Reproducing the solar luminosity is the ultimate requirement to all stellar evolution models. In other words, the total solar irradiance is used to calibrate models of stellar evolution. The energy production in the core of a main-sequence star is balanced by the radiant emission at the stellar surface. Since the energy production rate as well as the radiant emission strongly depend on the temperature of the core and surface, respectively, accurate measurements of the solar luminosity provides a direct link to the temperature not only at the solar surface but also in the solar core.

Latitudinal irradiance scans also allow assessment of latitudinal temperature gradients which might be linked to meridional flows.

1.2.4 Q4: How does magnetic activity shape the structure and evolution of the polar solar corona and how does it affect the Earth?

In addition to measurements of photospheric and subsurface motions and magnetic fields, it is the first opportunity to observe the outer solar atmosphere of the polar region in detail.

Coronal Structures and Activity in Polar Regions

The Japanese solar physics community monitored the brightness of the solar corona at a height above the solar limb by small ground-based coronagraphs for 60 years covering five 11-year solar activity cycles (Figure 11). In the space program, the whole Sun was monitored in soft X-ray observations by the 2nd Japanese solar mission, *Yohkoh*, from 1991 to 2001 (Figure 12).

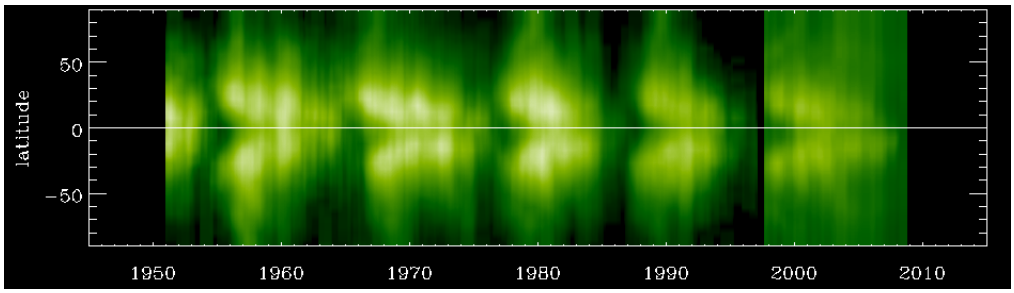

Figure 11. Coronal brightness variation in time-latitude diagram from the observation in the coronal green line (Fe XIV 5303) by the ground-based coronagraph at Norikura Solar Observatory (NAOJ)

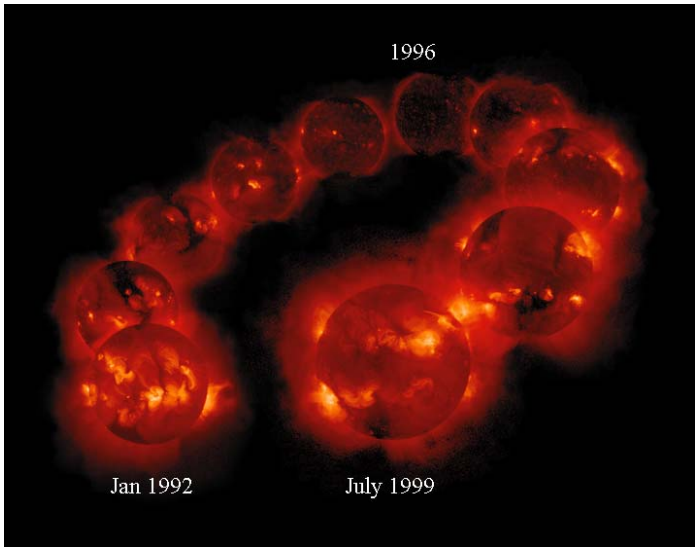

Figure 12. Cyclic variation of coronal structures in soft X-rays from *Yohkoh* (ISAS/JAXA)

Similar to the butterfly diagram of sunspot and surface magnetic fields, long-term coronal activity also shows the butterfly pattern in the time-latitude diagram. It has been well known since 1950's that there is a pole-ward migrating blanch in the diagram (Waldmeier 1957).

The polar regions of the Sun outside the solar maximum have a ray-like structure called 'polar plume.' The structure is well observed by white-light observations at the eclipse time or coronagraph observations in space. It is known from Skylab era that its electron temperature is slightly lower than the inter-plume region. The STEREO observations of polar regions with two view angles show where polar plumes observed with two coronal EUV imagers are rooted. However, the magnetic activity at the root could not be measured by a foreshortening effect by observing the polar region from the ecliptic plane, so that how these structures are formed has not been fully understood. Imaging observations of polar plumes from a vantage point in the SOLAR-C orbit will clearly address where and how they are formed. In addition to measurements of photospheric magnetic fields and imaging of transition region (TR) and corona, EUV imaging spectroscopy is of vital importance in revealing what basic processes are occurring at the roots of polar plumes and how plasmas in plumes move as results of the processes. One of the important measurements is to detect clear evidence of Alfvén waves in the polar plume or in inter-plume regions as we stress in the next sub-section of solar winds.

Near the solar maximum phase, the polar region is covered by many closed magnetic field structures with a ray-like shape at their tops, streamers. The phase of their appearance is near the time of polar magnetic field reversals. The coronal imaging observations from the SOLAR-C out-of-ecliptic orbit will clearly tell us how magnetic fields of these structures are connected at the photosphere and how these structures are formed near the solar maximum phase.

In addition to characteristic global magnetic structures in polar regions, small bipoles are also universally observed there. They were called X-ray bright points or coronal bright points that were first observed in an early sounding-rocket experiment with soft X-ray imaging telescopes. They are distributed all over the latitudes. From photospheric and coronal observations near the disk center, opposite magnetic polarities appear to be cancelling at the photospheric level beneath coronal bright points. It is believed that they are produced though magnetic reconnection in the corona by

interaction between opposite magnetic polarities that have already seen above the photosphere, not as a direct emergence of a small bipolar structure. The elemental process occurring up to the mid latitudes is being investigated by *Hinode* with its high-spatial resolution in a narrow field of view. The small bipoles are replenished rapidly with time and the total magnetic flux exceeds those brought from the global magnetic activity showing a quasi-periodic activity of roughly 11 years. The occurrence frequency of the bright points measured in low-latitude regions is found to be roughly constant in contrast to the normal solar magnetic activity that has a quasi-periodic 11-year cycle. The low-amplitude or almost constant cyclic behavior may be the presence of a different dynamo action that locally functions. It is not clear at present that the emergence rate of such bipoles in polar regions is the same as that in low latitudes. A direct observation with less foreshortening effect from the out-of-ecliptic orbit with less overlap by foreground and background corona will clearly answer the behavior of small bipoles in polar regions.

Hinode high-cadence X-ray observations have shown that polar regions are more dynamic than expected from the extension of *Yohkoh* X-ray observations as revealed from a higher occurrence frequency of coronal jets (Cirtain et al. 2007). *Hinode* has also revealed from a high-resolution vector magnetic field measurement that the formation of coronal jets in a polar coronal hole is found to be associated with newly discovered photospheric kG concentration of polar magnetic fields through magnetic reconnection (Kamio et al. 2009). Such events may produce Alfvén waves that are thought to be important to the acceleration of the fast solar wind. EUV spectroscopy with enhanced sensitivity will reveal the coronal dynamics in polar region.

Solar Wind

Supersonic plasmas flow into interplanetary space from the Sun as the solar wind. Many in-situ observations in the ecliptic plane have shown that the speed of the solar wind ranges from 300 to 800 km/s. Timing analysis of the fast solar wind (600-800 km/s) with full-disk X-ray images and global open magnetic field structures of the Sun have revealed that polar coronal holes and those extended from polar regions to lower latitudes are the source of fast solar wind. The solar wind speed measured by Ulysses whose orbit is largely inclined to the ecliptic orbit clearly showed that there is a latitudinal variation in the solar wind speed and that the speed is bi-modal in the solar minimum phase, that is, the slow wind with outflow speed of 300-400 km/s in low latitudes and the fast wind of 600-800 km/s in high latitudes (McComas et al. 2003, 2008; Figure 13). It is also known from Ulysses that the slow solar wind also appears in the high-latitude region near the solar maximum phase (Figure 13). It is widely accepted that the fast solar wind is so fast that the speed cannot be explained by Parker's thermally driven wind model alone. An additional energy input needs to be given to the plasma flow. The interplanetary scintillation (IPS) observations show that the acceleration of the solar wind is almost finished within 30 solar radii.

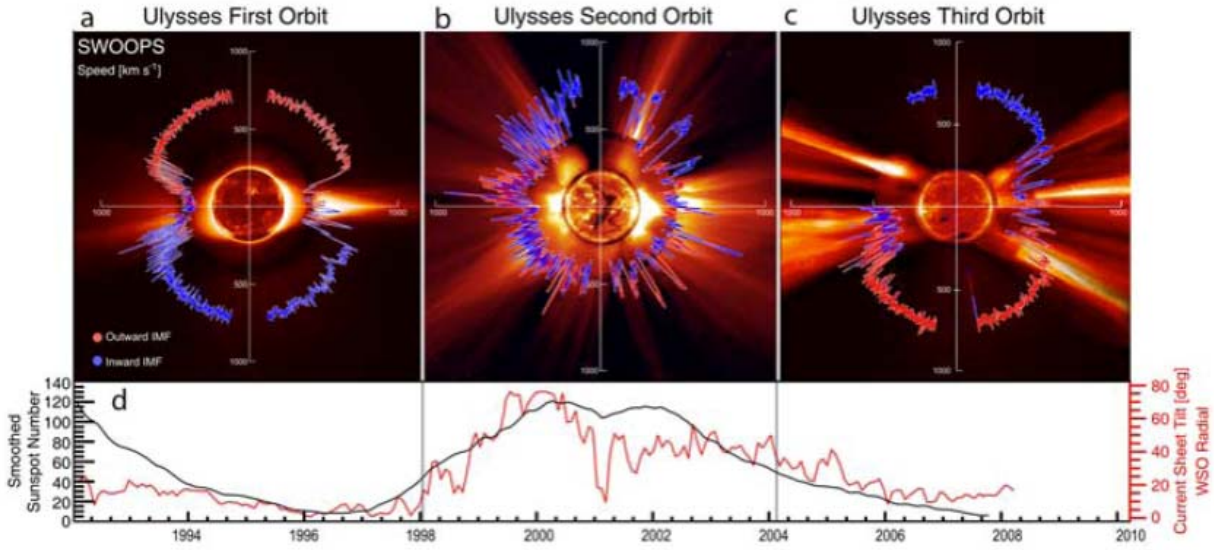

Figure 13. Solar wind velocity measurements by Ulysses (McComas et al. 2008)

There were two categorized candidates for the mechanisms of fast solar wind. One is a fast jet produced at the transition region or low corona, and the other is the acceleration by waves in the corona. The possibility of the former disappears after SOHO observations because the high-speed jet is not universally observed in the EUV imaging and spectroscopic observations in the transition region and low corona and because the acceleration of the flow speed at the location between the low corona and a distance of 30 solar radii becomes mandatory from the tracking of white-light coronal structure seen in the coronagraph (Sheeley et al. 1997) and from the evaluation of wind speed by Doppler dimming technique (Cranmer et al. 1999). The unexpectedly larger number of jets in polar coronal holes has been found by *Hinode* X-ray imaging observations (Cirtain et al. 2007; Figure 14). Although it may contribute to some fraction of the total mass with a million degree for the fast solar wind, it cannot explain the acceleration of the solar wind in the most inner heliosphere within 30 solar radii.

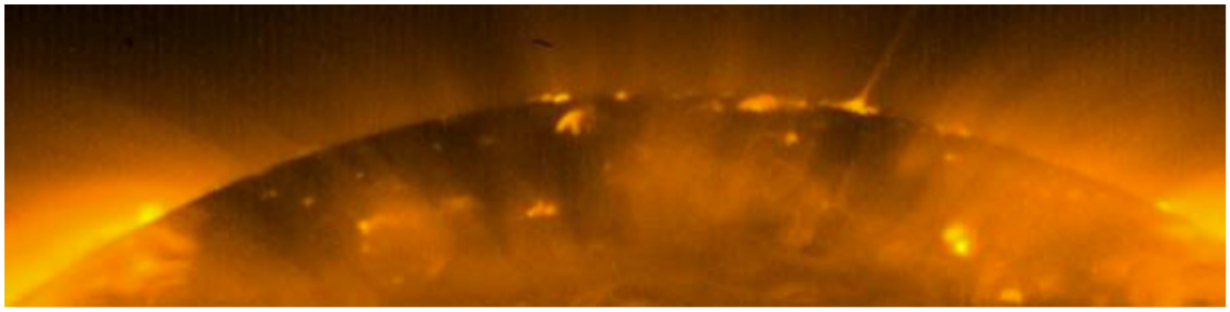

Figure 14. North polar coronal hole observed with *Hinode* XRT showing a coronal X-ray jet

One of the most promising mechanisms is acceleration of the wind plasma by Alfvén waves. The wave itself has normally been found in solar wind plasmas by in-situ measurements since the early space age (Belcher and Davis 1971). The source of the Alfvén waves is not well understood. It may be a wave simply produced by the photospheric motion of magnetic field structure by granule motions or a wave created by magnetic reconnection in the low corona. A high-speed solar wind is reproduced in Suzuki & Inutsuka (2005) by the photospheric lateral motion of the magnetic field. However, clear evidence of Alfvén wave with sufficient energy flux has not been found in the polar

coronal hole. The wave signatures near the base of polar coronal holes that have been reported are mostly identified as slow-mode waves. One of the signatures for the presence of Alfvén wave near the base of the corona is enhanced line broadening of the coronal emission lines that are always observed in polar coronal holes. If it is found that this broadening is actually caused by Alfvén wave, where the energy flux of Alfvén waves created and what amount of energy flux Alfvén waves have could be understood. One way is to look at the polar region with an imaging spectrometer from various angles or to look at the same point stereoscopically with two imaging spectrometers that locates at different heliocentric latitudes. For this type of observation, higher spatial and spectral resolutions than those realized as SOHO SUMER and *Hinode* EIS is not required.

The solar wind is largely accelerated to the coronal sound speed near 2-3 solar radii and become supersonic beyond that point. In the upper part of the corona at a radial distance above ~2 solar radii, the hydrogen Lyman alpha line (H I) at 1216 Å shows a spectrum of very wide line width. This was first discovered by the sounding rocket experiment in l979 (Kohl et al. 1980). The emission mechanism is the resonance scattering of photons nearby the Lyman alpha wavelength by a small amount of neutral hydrogen in the corona, and was identified in Gabriel (1971). A similar line profile is seen in ionized oxygen resonance lines O VI at 1032 Å and 1037 Å (Figure 15). The number of scattered photons depends on the outflow speed of each hydrogen or ionized oxygen atom that absorbs a photon and re-emits. Faster plasmas scatter the smaller number of photons (Doppler dimming). The bulk flow speed of the solar wind plasma was evaluated from the scatted photons by SOHO UVCS in the inner corona that cannot be accessible by IPS observations. The cause of the largely enhanced line broadening is not fully understood. One definite contribution is from the line-of-sight component of the solar wind bulk outflow and the other is from the local mass motion of atoms. The local mass motion consists of the thermal Doppler motion and some additional mechanical motions. The latter contribution contains information of the heating and acceleration of solar wind plasmas.

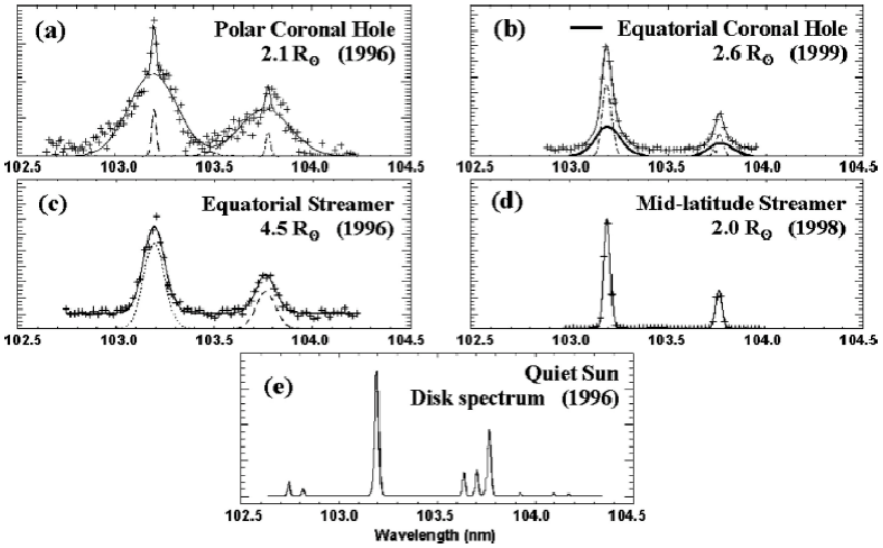

Figure 15. Enhanced emission-line broadening at observations above coronal holes with SOHO UVCS (from Kohl et al. 2006).

Largely enhanced emission-line widths have been found in O VI observations with SPARTAN and SOHO UVSC (Figure 15). The line width implies that there will be large ion mass motions

perpendicular to the line-of-sight direction. It is sometime referred to be 100 MK at height above 2 solar radii, while the electron temperature at that height is about a million degree. The enhanced kinetic temperature is interpreted as a perpendicular motion of ions to the magnetic field line ($T_\perp$), and its highly anisotropic kinetic temperature ($T_\perp/T_{//}$ ~100 >>1) is due to the heating by some mechanisms. As a potential mechanism, the ion cyclotron resonance heating has been proposed (McKenzie et al. 1995; Cranmer et al. 200?). The mechanism requires a high-frequency Alfvén waves of 10^4 Hz in the corona, which cannot be expected by the low frequency (0.001-0.01 Hz) photospheric granule motions. The estimate of $T_\perp$ on O VI observations depends on the model outflowing atmosphere in polar coronal holes. A solution to satisfy the UVCS observation is possible for simple isotropic kinetic temperature ($T_\perp=T_{//}$) cases (Raouafi and Solanki 2006) and for reduced anisotropic ($T_{//} < T_\perp < 10\ T_{//}$) cases (Nakagawa 2007). Observations of polar coronal holes from different helio-latitude by the SOLAR-C Plan-A spacecraft from out-of-ecliptic orbit or stereoscopic measurements with a spacecraft in a low Earth orbit or at L_1 Lagrangian point will resolve this discrepancy and leads to correct understanding of motions of ionized atoms with different mass from hydrogen. The global magnetic-field structure inferred from the SOLAR-C magnetic field measurement and coronal imaging from a high-inclination vantage point will also become a help for understanding the magnetic structures in polar coronal holes as a model input.

The solar wind speed in the polar region changes in the solar cycle as shown in Figure 13. When the SOLAR-C spacecraft is in the final orbit, the spacecraft can see each polar region for a few months per year in a good condition above 30° from the solar equatorial plane. The change of flow speeds at the coronal base from the open magnetic-field region in each polar region can first be monitored during the rapid change in the polar reversal phase. The flow speed as a function of evaluated expansion factor of magnetic field structures in the polar region, which is considered to be a key factor for the fast wind speed, may be observed by SOLAR-C.

Coronal Mass Ejections & Disturbance

Coronal Mass Ejections (CMEs) are the most powerful source of the heliospheric disturbances and the primary cause of the geomagnetic storms. Understanding and predicting their initiation, evolution and interaction with the planetary atmosphere is one of the most important topics in solar physics and the space weather studies. The other source of geomagnetic disturbance is the Co-rotation Interaction Region (CIR), the large-scale plasma structures generated by the interaction of fast and slow solar winds. The recurrent MeV-ion events and the decrease of the galactic and anomalous cosmic ray intensity are also associated with CIR.

Initiation of CMEs and acceleration of the solar wind in the lower corona are being investigated in detail by *Hinode*, using the combination of photospheric and chromospheric observations by the SOT and coronal observations by the EIS and XRT. In order to investigate the later evolution of CMEs and CIRs in the inner heliosphere, it is necessary to have continuous imaging observation that covers from the outer corona to the interplanetary space.

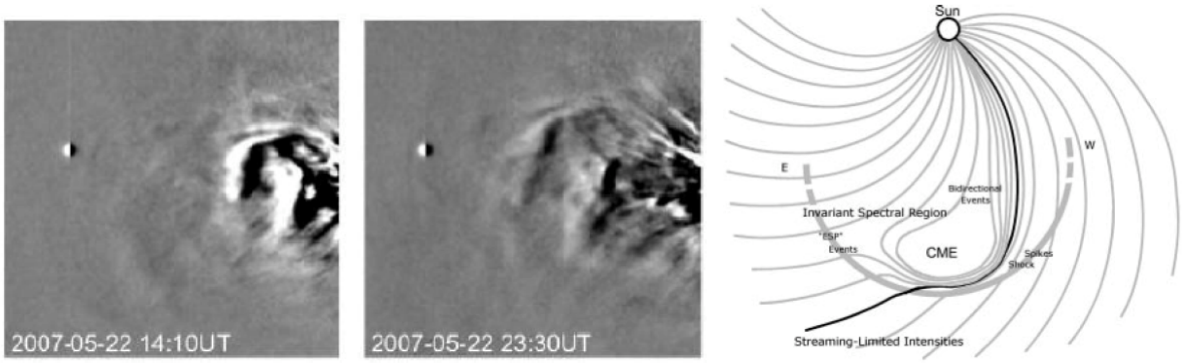

Figure 16. (Left and Middle) Evolution of a CME event observed with STEREO/HI-1 (from Harrison et al. 2009). (Right) Overhead view of the CME travel in the Sun-Earth interplanetary space (from Reames 1999)

The STEREO Heliospheric Imager instruments clearly demonstrated that CMEs and CIRs near 1AU and beyond can be detected by such instruments (left and middle panels in Figure 16; Harrison et al. 2009), and provided the first stereoscopic view of the solar corona and the inner heliosphere. With a STEREO/HI-like imaging instrument on board SOLAR-C/Plan-A, we will be able to obtain the first overhead view of the heliosphere, which has been often drawn as "cartoon models" by many researchers (right panel in Figure 16). It will allow us, for the first time, to investigate the evolution of CMEs and CIRs in the background Parker-spiral solar wind.

Combination of the context heliospheric image from SOLAR-C/IHI and the in-situ plasma measurement in the ecliptic by a spacecraft such as ACE, WIND, GEOTAIL and Cluster will be of great synergy. For example, the basic structure of CME is believed to be twisted flux rope that is either already formed before eruption or generated during the eruption by the post-eruptive reconnection (Forbes 2000). However, it has been pointed out that the interplanetary CMEs (ICME) observed by in-situ instruments at 1AU often show more complicated structure without well-defined flux rope (Richardson and Cane 2004). With the overhead view of the CMEs from SOLAR-C, we can tell where in the CME the in-situ instruments are observing, thus allowing the interpretation of the in-situ measurements in the global context.

The overhead view also has a great impact from the space weather point of view, as we will be able to see what part of the CMEs and CIRs are going to hit the Earth that allows more reliable prediction of the solar wind properties at the Earth.

Solar energetic particles (SEPs) associated with flares and CMEs and cause significant damage of the spacecrafts and disruptions of the human activities in the space. Moreover, acceleration of energetic particles is one of the most fundamental processes in the space and astrophysical plasmas. Understanding the production of SEPs and their propagation to the Earth is therefore one of the most important subject in the solar and heliospheric physics from both practical and academic points of view. Indeed, the solar corona, interplanetary space and the Earth's magnetosphere provide powerful and complementary laboratories for particle acceleration. While imaging of the solar corona shows the global change of the magnetic topology, in the magnetosphere, detail microscopic plasma processes can be observed by the in-situ measurements. On the other hand, with the out-of-ecliptic heliospheric imager and the other in-situ instruments, the interplanetary space provides a unique laboratory in which one can see both the global dynamics and morphology and the microscopic plasma processes.

Phenomenologically, SEP production can be classified into two categories, one associated with solar flare in the low corona (or more physically, magnetic reconnection), and the other associated with CME-driven interplanetary shocks. SEPs are usually observed at 1AU after they escape from the acceleration site and propagate, primarily along the interplanetary magnetic field, to the spacecrafts. Note that shock acceleration also is believed to be occurring in many astrophysical phenomena, such as generation of the galactic cosmic rays (GCRs) in the supernova shocks and gamma-ray bursts.

SOLAR-C/HI can address this issue by providing the global context of the interplanetary space in which acceleration and transportation occur. From the overhead view of the CMEs we can measure the mach number and, with an assumption of Parker-spiral-like ambient solar wind, the angle between the shock normal and the ambient magnetic field in the upstream. Also by assuming the Parker spiral, one can determine the magnetic connection of the shock front and the spacecrafts observing the SEPs in the ecliptic. Using this information and a model of SEP transportation, one can determine where in the CME shock the SEPs come from, thus allowing the comparison of the acceleration models and observations.

In-situ Measurements in the Inner Heliosphere

The past solar activity has been investigated by cosmogenic isotopes such as ^{14}C and ^{10}Be. These are created by the interaction between atoms in the Earth's atmosphere and cosmic rays in a certain energy range (~ a few GeV or below). These cosmic rays mostly arrive at Earth through the heliosphere during a course of a long travel in our galaxy. Due to the change of magnetic field structure in the heliosphere according to solar cycle variations, the number of the cosmic rays suffers from significant modulation. The transport process of cosmic rays in the heliosphere was first shed light on by Parker (1965). The theory describes the time evolution of the cosmic ray distribution function by processes of (1) convection and adiabatic energy change by solar wind velocity, (2) turbulent irregularities, and (3) gradient, curvature, and current-sheet drift. The basic formulation is still valid. However, there are uncertainties in various parameters.

Ulysses has executed the fist measurements of cosmic rays at high heliocentric latitude of 80°. It was expected that the cosmic ray intensity would increase an order of magnitude compared by the measurement near the ecliptic plane because the local interstellar cosmic rays can travel to the inner heliosphere along the magnetic field without significant modulation. In contrast to the theoretical expectation, Ulysses found that the cosmic rays increase only a few ten percents from ecliptic to the high latitude during the solar minimum. This indicates enhanced diffusion by turbulent irregularities in the high latitude. Thus, the transport model of cosmic rays in the heliosphere is not consistent with the Ulysses observations. The maximum inclination angle of 33° from the ecliptic plane in the SOLAR-C Plan-A orbit is smaller than that of 80° in the Ulysses orbit. However, a fast scan with a constant period of a half year at 1 AU distance from the Sun is an advantage in the SOLAR-C Plan-A orbit for the scan range from the northern maximum to southern maximum latitude, and may have an advantage of investigating how the particle counts vary with the solar activity cycle in a fixed observing condition. The measurement may produce unique data set to enhance the value of long-term data on the variation of cosmogenic isotopes that record the past solar activity. Without this measurement no progress is expected from observations for the transport of cosmic rays in the heliosphere in the coming decades.

2. Scientific Requirements

2.1 Scientific Requirements

2.1.1 Requirements for Helioseismology Observables

The success of global helioseismology, which is centered at precise measurement of the solar eigenfrequencies and inversion of these frequencies, is well documented. In particular, mapping the solar differential rotation (Figure 7) and meridional flow (Figure 8) throughout the low- to mid-latitude convection zone had a great impact on our understanding of the solar dynamo.

One inherent limitation of global helioseismology comes from inverse analysis based on the linear perturbation theory, and the symmetry of the global eigenfunctions; the structure inversion is primarily about estimating the spherically symmetric component of the thermal structure of the sun (even inversions for aspherical components of the thermal structure of the sun is accessing only those components that are axisymmetric and north-south symmetric), and the rotation inversion is about measuring the axisymmetric, north-south symmetric component of the solar internal flow. Moreover, the sensitivity kernels for rotation inversion, derived from the eigenfunctions, do not have large amplitude in higher latitude region.

Local helioseismology, based on local measurement of wave propagation, particularly wave travel times, is better suited for revealing local structure free of any kind of symmetry that are mentioned in the above. Local helioseismology has already been successful in measuring near-surface component of meridional flow (Figure 8), which is the key ingredient in flux-transport dynamo, up to around 60° latitude (Giles et al. 1997). Extending the measurement to higher latitudes is one of the main scientific targets of SOLAR-C Plan-A.

Thus there are two main objectives of heliseismology observations from an inclined orbit: 1. *High-latitude local helioseismology*: measure local wavefield in high-latitude region better than from within the ecliptic place, for local-helioseismology analyses of various flows in the near-surface (and if possible, deeper) layers, such as meridional flow. 2. *Multi vantage-point helioseismology*: in combination with observing facilities in the ecliptic plane, observe waves with large skip angles better, for helioseismology analyses of deep interior, such as mid-latitude tachocline regions. The first objective is more promising in producing important results, whereas the second objective is more challenging.

Helioseismology requires long continuous observing periods at a high time cadence in order to resolve the various spatial and temporal scales associated with processes of generation and dissipation of solar magnetic fields. These scale range from supergranulation, which defines the magnetic network and is a primary source for magnetic field diffusion and has a typical spatial scale of 30 Mm and lifetime of about 1 day, and larger-scale dynamics of active regions occupying 50-100 Mm and evolving on the scale of a week, to the global meridional and zonal flows occupying the whole convection zone 200 Mm deep and varying with the solar cycle on the time scale of a year.

These three fundamental scales of solar dynamics and activity define three basic observing patterns that are needed to achieve the primary objective above: relatively short (8 hour long) but high-resolution (512×512 pixels) time series to investigate the structure and dynamics on the

supergranular and magnetic network scales; longer (7-14 days) and high-resolution (512×512 pixels) series to follow the evolution of individual active regions (particularly, on the far side of the Sun in conjunction with Earth-side observations), and long time period (36-72 day) low resolution (256×256 pixels) observations to investigate the global dynamics and circulation of the convection zone down to the tachocline by both local and global helioseismology techniques.

All these observing programs require a 1 minute cadence for the Dopplergrams. However, a strict temporal continuity requirement (95% coverage) is required for 8-hour chunks of these programs. The longer observing programs may have gaps. However, the total coverage should be at least 70-80%, in particular, for the global helioseismology 36-72-day runs in order to prevent the aliasing problems in the measurements of mode frequencies and frequency splitting. The precision of the frequency measurements is inverse proportional to the square root of the observing time. Currently, 72-day runs are used in the SOHO/MDI Structure program that is similar to the low-resolution (256×256 pixels) SOLAR-C program. These runs provide inversion results for solar structure, asphericity and rotation through the whole convection zone, tachocline and outer radiative zone. Shorter, 36-day runs will still provide new results for the convection zone sufficient for studying the torsional oscillations and other global variations. However, the ability to resolve the tachocline structure and dynamics will be greatly reduced. The investigation of the solar-cycle variation in the tachocline region may require 12-month long averaging of the frequency measurements. The minimum science requirement for exploring the solar-cycle variations in the polar regions is to have two or three 36-day runs per year.

Table 2. Helioseismology Observing Requirements

Measurement Objective(s)	Technique	Length of observation	Image size (pixels)	Image cadence
Differential rotation and torsional oscillations at high latitudes, sub-surface polar jets	Global	36-72 days	256×256	1 min
	Local	8 hrs	512×512	1 min
Meridional circulation, latitudinal and longitudinal structures, secondary cells, relationship to active longitudes, magnetic flux transport	Local	8 hrs	512×512	1 min
Supergranulation and large-scale convection patterns in polar regions (super-rotation, wave-like behavior, network, flux transport, relationship to coronal holes)	Local	8 hrs	512×512	1 min
Structure and dynamics of the high-latitude tachocline (oblateness, flows)	Local	36 days	256×256	1 min
Tomography of the deep interior: stereoscopic observations (SOLAR-C-SDO, SOLAR-C-GONG)	Local (time-distance, holography)	36 days	256×256	1 min

The different measurement objectives, the observing technique and the observing requirements are listed in Table 2. Global helioseismology, which assumes symmetry about the rotation axis of the Sun, requires a very accurate determination of the frequencies of the Sun's acoustic modes of to determine the longitudinal rotation as a function of depth; the longest observation times (36-72 days of continuous, 70-80% coverage data) are needed to determine the frequency and frequency splitting of solar oscillation p-modes of low angular order, m. These modes, in particular, zonal m=1 modes, propagate into the polar regions and provide the information about the polar structure and dynamics. The current ecliptic-viewpoint observations do not provide measurements sufficiently accurate for helioseismic inversion of the solar structure and rotation in the polar regions. It is important to complement the SOLAR-C observations with ecliptic-viewpoint data in order to infer the structure and dynamics of the whole Sun, from the equator to the poles.

It can be seen from the table that some of these measurements require high latitude viewing for many days at a time. This was the driving requirement for choosing an orbit inclination with the highest possible inclination. The high-latitude viewing will provide a unique opportunity to study the dynamics of meridional flows and rotation in the polar regions and search for deep longitudinal structures in the tachocline by local helioseismology. In addition, the high-latitude orbit will allow us to obtain better coverage of the deep polar regions using the observing scheme with two vantage points, SOLAR-C and ecliptic viewpoint helioseismology instrument.

The required telemetry for the helioseismic observations is case dependent. However, it is obvious that the reduction of the data by on-board processing is mandatory. For a measurement of Doppler velocity map with a simultaneous measurement of line-of-sight magnetic fields, two polarization states of I +V and I-V need to be observed at four wavelength positions for a good estimate of the line-of-sight magnetic fields. This methodology was used in *Hinode* filtergram observations. The eight images obtained at eight observing times can be reduced to two index maps by simple arithmetic operations, each can be converted to Doppler velocity and line-of-sight magnetic field by a known non-linear function. If we need Doppler velocity maps of 512×512 imaging points every 1 min, ~13 kbit/s data rate is required for the data compression efficiency of 3 bit/s (512 ×512 pixel × 3 bit/pixel /60 s =13,107 bit/s) that is achieved in *Hinode*. For the case of local helioseismology that requires both a large field of view and high-spatial resolution, 1024×1024 imaging points may be necessary, and the required data rate becomes ~51 kbps (1024×1024 pixel × 3 bit/pixel /60 s =52,429 bit/s).

2.1.2 Requirements for Magnetic Fields Observables

Along with the Dopplergrams, full-disk line-of-sight magnetograms of 1024x1024 pixels will be taken every 5 (TBD) minutes to observe the response of the magnetic field to the surface, sub-surface and interior flows. Together, these observations will be used to study phenomena such as the evolution of active regions, flux transport and the solar cycle field reversal. SOLAR-C, complemented by near-Earth magnetograph observations, will enable us to follow the evolution of active regions continuously for much longer than the half-solar rotation now possible. Full-sun vector magnetic field observations shall be done every 60 min (TBD) or high-cadence observations of vector magnetic fields shall be possible for a 4×4 (TBD) arcmin field of view.

The required data rate for line-of-sight magnetograms of 1024x1024 pixels of 5 minutes cadence is about 10 kbps (1024 ×1024 pixel × 3 bit/pixel /300 s =10,486 bit/s). When four Stokes polarization

states of I, Q, U, V are obtained at four wavelength positions, 16 imaging data need to be downloaded to the ground. 2048×2048 pixel vector magnetograms every 2 hours requires ~27 kbps (2048 ×2048 pixel × 3 bit/pixel × 16 images/7200 s =27,962 bit/s). For the active region monitor by vector magnetic fields of 256×256 pixel imaging points, the data rate of 51 kbps (256×256 pixel × 3 bit/pixel × 16 images/60 s =52,429 bit/s) is required for cadence of 1 minutes.

2.1.3 Requirements for TSI Observations

The fastest approach to reach the science goals for TSI measurements is to compare a latitudinal scan of the solar irradiance to contemporaneous measurements from in-ecliptic spacecraft from the long-term TSI monitoring programs, such as SORCE/TIM and PICARD/PREMOS or their successors. A slightly more demanding approach consists in a self-contained statistical analysis of several latitudinal scans to detect latitudinal trends in irradiance. Both approaches would benefit form observations at higher heliographic latitudes but extrapolation of trends in the SOHO/VIRGO measurements, which cover ±7°, suggests that 30° is sufficient to answer the above questions.

The SOLAR-C TSI instrument produces the on-source and off-source irradiance data by the periodic operation of a shutter located in front of one of cavities. The average and peak data producing rates are ~2 kbits/s and ~4 kbits/s after the data compression. The full FOV is about 5° and there is a 15 arcmin pointing tolerance. This instrument is assumed to be continuously operated in the SOLAR-C out-of-ecliptic orbit after the nominal operation. There may be a request of a special operation to do an intentional offset pointing for instrument calibration.

2.1.4 Requirements for EUV imaging and Spectroscopy Observables

For the imaging of transition-region (TR) dynamics, a band at 304 Å is suitable. Polar plumes are visible in a band at 171 Å and 195 Å. Hotter coronal plasma components in coronal bright points and active regions are observed in a band at 335 Å. These are observed by a telescope consisting of multilayer mirrors that has a spatial resolution of ~2 arcsec by ~1 arcsec spatial sampling. The field of view covers the whole Sun when the spacecraft points to the disk center. One of these bands is observed at a time. Wide slit observations of EUV scanning spectrometer may supplement the imaging of the TR and corona, but the images obtained with the wide slit are not sharp due to the blurring in the spectral direction. The wide slit observation cannot be used for the stereoscopic observations with a similar telescope in other line-of-sight directions. In the case of selecting a grazing-incidence telescope as a SOLAR-C coronal imager, observations of polar plumes may be performed in a low-contrast condition and the TR observations become impossible. A nominal operation is a combination of the full-disk observation at ~1 hr interval low cadence and smaller field-of-view observations with a higher cadence of few min. A fast observation consuming all allocated telemetry in a short time needs to be supported. ~20 kbps data recording rate is necessary when a data compression of 1.5 bits/s is considered.

Emission line spectroscopy with focusing optics is required to measure flows of solar-wind source region and to detect a signature of Alfvén waves that is a promising candidate to accelerate fast solar wind. A candidate of wavelength is in EUV. Although EUV instruments are relatively heavy, the SOLAR-C EUV scanning spectrometer needs to be achieved in a lighter weight condition

because the total payload mass is limited. It is possible to enhance the instrument sensitivity of a small EUV spectrometer that is better than that of SOHO/SUMER (*Hinode*/EIS) by reducing the number of reflections (or reducing the filter components that shut the visible light). A higher sensitivity by more than a factor of 5 increase from the current space instruments is required. In addition to measurement of emission-line intensity, a spectral resolution similar to EIS and SUMER is needed to evaluate the dynamics of hot plasmas. The FOV center needs to be changed by moving an internal optics like SUMER, which could change the FOV in the north-south direction to investigate the outer region of polar coronal holes. A nominal image size of 256x256 pixel data points with 10 sec cadence produces ~20 kbps data when the data are compressed in a 3 bit/pixel lossy data compression like JPEG2000.

2.1.5 Observables of inner heliospheric imaging (Optional)

The imaging data of the inner heliosphere in the visible-light range are obtained by periodic exposures that produce a huge data volume. The exposure duration of ~1 min is a typical exposure, and the on-board summation of 60 frames, so that the image producing rate is one imager per 60 min. The final image size after the binning is 1024x1024 with 16 bit depth at each image point. Assuming 40 percent data compression, the final data producing rate is about 2 kbps. The FOV size is 60° to cover a large inner heliosphere and the FOV center point to a point above the solar south pole with an offset angle of ~45° (TBD) from the disk center. This setting of the instrument gives an overhead view of the Sun-Earth space in the ecliptic plane when the spacecraft is in the northern heliosphere. The spacecraft needs to rotate by 180° around the spacecraft Z axis if the Sun-Earth space in the ecliptic plane should also be observed when the spacecraft is in the southern heliosphere.

The following objects are contained in the observed data: solar wind structures and CME (via scattered light by electrons in the heliosphere), diffuse Zodiacal light (via scattered light by dust particles in the heliosphere), stars, planets of our solar system, comets, and asteroids. The brightest object is planets as a point source and scattered light by dust particles as a diffuse source. To determine a dust distribution from the measurement of Zodiacal-light brightness, a special observation in which the spacecraft Z axis is largely offset to the disk center may be required. Since it is strongly related to the safety operation of spacecraft, a risky attitude maneuver shall be avoided.

2.1.6 Observables of in-situ measurements (Optional)

Not studied in detail. The measurement of solar wind velocity for main elemental species will be mandatory. The in-situ magnetic field will also be a basic parameter, but the level of ~1 nT magnetic field at 1 AU may not be measured by the strong magnetic fields from permanent magnets used in ion engines when the SOLAR-C orbit is formed with help of solar electric propulsion system.

2.1.7 Summary of Required Data

Table 3 summarizes the data required for SOLAR-C Plan-A.

Table 3. Data required for SOLAR-C Plan-A

Measurement		Wave-length (Å)	Spatial sampling	Image Size (Pixels)	Number of images transmitted	Cadence	Data rate (kbps)
1	Photospheric line-of-sight Doppler velocity: Global Helioseismology	Visible	4.0 arcsec	512×512	1	1 min	*13
2	Photospheric line-of-sight Doppler velocity: Local Helioseismology	Visible	1.0 / 2.0 arcsec	1024 ×1024	1	1 min	*51
3	Photospheric line-of-sight magnetic field	Visible	1.0 arcsec 2.0 arcsec	2048×2048 1024 ×1024	1	10 min	*10 *5
4	Photospheric vector magnetic field	Visible	1.0 arcsec	2048×2048 256×256	16	8 hours 10 min	*7 *5
5	Imaging of Chromosphere	Visible (TBD)	1.0 arcsec	2048×2048	1	1 hour	#3
6	Imaging of TR and Corona	EUV/X-ray	~1.2 arcsec ~2.4 arcsec	2048×2048 1024×1024	2	1 hour 5 min	#3 #20
7	Imaging spectroscopy of Chromosphere, TR, and Corona	EUV	~1.0 arcsec	spatial×spectral 256×256	1	10 sec	*19
8	Monitoring TSI	-	-	-	-	1 min	2
9	Heliospheric imaging [option]	visible	0.03°	1024 ×1024	1	1 hour	*1
10	In-situ (TBD)	-	-	-	-	-	~1

*(#)Data compression down to 3 (1.5) bit/pixel is assumed

2.2 Science Payload

Table 4 shows candidate payloads for SOLAR-C. The description of each payload is shown in the following subsections.

Table 4. SOLAR-C Plan-A Model Payload

HAI (Helioseismic Activity Imager)		MDI+electronics 57 kg
Weight	65 kg	HMI+electronics
Aperture: 12.8 cm		+ harness 73.5 kg
Detector: APS or Backside illuminated CCD		
Sampling: 0.5 arcsec/pixel (TBD)		
Detector format: 4K×4K (TBD)		
Wavelength: 5000-8700 Å		
LIM (Luminosity and Irradiance Monitor)		2 PMOD+electronics in
Weight	5.0 kg	VIRGO: ~5 kg
Number of cavities	≥3	TIM(4 cavities): 10 kg
EAI (EUV Activity Imager)		STEREO EUVI
Weight	12 kg	telescope alone: 7.7 kg
Ritchey-Chretien telescope with Mo/Si mirrors		
Detector: APS or Backside illuminated CCD		
Sampling: 1.2 arcsec/pixel		
Detector format: 2K×2K (TBD)		
Wavebands: 171, 195, 304, 335 (all TBD) Å		
ESS (EUV Scanning Spectrometer)		
Weight	30 kg	
Two reflection system: offset parabola + concave grating		
Spectrometer with a factor of 4 (TBD) magnification		
Detector: intensified APS or intensified CCD detector		Use of MCP
Sampling 0.75 arcsec/pixel (TBD)		148cm focal length
Detector format: 4K(spectral)×1K(spatial) TBD		
Waveband (TBD):		
IHI (Inner Heliospheric Imager; **Optional)**		STEREO HI-1+HI-2
Weight	8.0 kg	+Electronics: 13.8kg
Detector: APS or Backside illuminated CCD		
Sampling: 0.03 deg/pixel		
Detector format: 2K×2K (TBD)		
Others (In-situ Measurements etc.)		
Weight	α kg	
Mission data processor if required		
Weight	β kg	
Total weight (130 kg tentatively allocated for payload)	120+α+β kg	

2.2.1 Helioseismic and Activity Imager

This instrument observes the Sun in the visible light for imaging the Sun in the continuum and at absorption lines, for acquisition of the helioseismic information from Doppler velocity observations, and for mapping the photospheric magnetic fields. It consists of a refractive telescope, a polarization modulator, a tip-tilt mirror, a narrow band tunable filter, and a mechanical shutter, and a 2D imaging camera. The narrow bandpass filter has a bandpass of 100-200 mÅ in full width at

half maximum (FWHM), and its central wavelength can be tuned in 5000-8700 (TBD) Å. A similar type filter with a wider bandpass of 1 Å FWHM was operated for imaging the green-line (5303) corona for 10 years at a ground-based observatory in Japan.

The baseline detector is a large-format CCD camera with 4K×4K (TBD) pixels. When a scientific grade CMOS detector is available, it is better to be adopted from the viewpoint of radiation hardness in the space environment.

The whole-sun area has to be observed in most of the time because the Doppler velocity observations for helioseismology will mostly be running except for some special operations.

The baseline data recording rate of this instrument is 50 kbps. When one of data is compressed to 3 bits/pixel average, three types of data of 512×512 pixels, magnetograms, Dopplergrams, and continuum image, can be obtained every 1 min.

Figure 17 shows the schematic optical diagram of the instrument. One of programmatic difficulties in developing this instrument is to realize a narrow band tunable Lyot filter that is being developed to raise TRL. When it is difficult to be developed , the use of Michelson interferometer with a wider band Lyot filter like SOHO/MDI and SDO/HMI observing a single absorption line or a Fabry-Perot filter may become a fallback plan.

The selected line for the Doppler and magnetic field measurement is a TBD line at TBD Å. Ni I 6768 Å (Fe I 6173Å) was selected for SOHO/MDI (SDO/HMI).

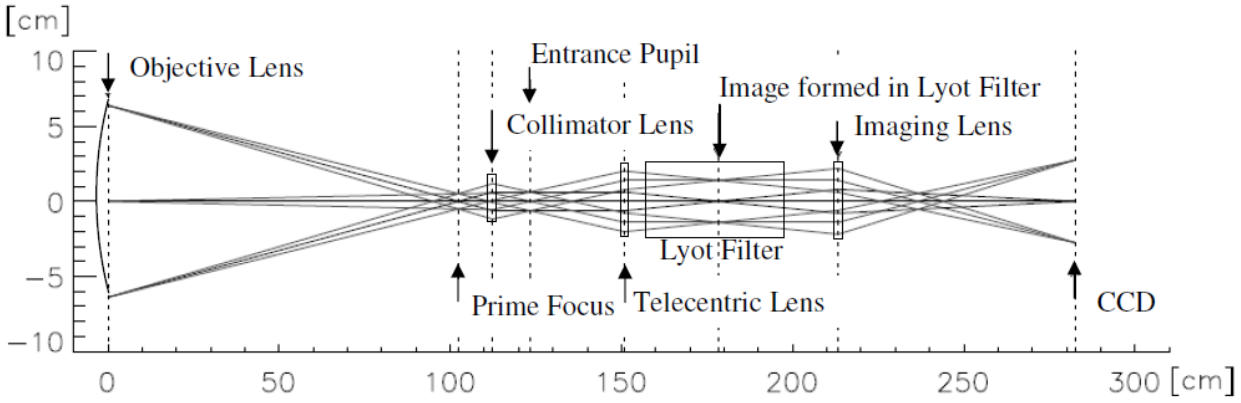

Figure 17. Schematic optical diagram of HAI conceptual design.

2.2.2 EUV & X-ray Spectroscopic Imaging Telescopes

A fast cadence imager is needed for tracking the evolution of dynamic events in the outer solar atmosphere. The SOLAR-C Plan-A is not a mission targeting to resolve elementary structures. It will be sufficient to cover the whole Sun corona with a range of extended corona above the limb of the Sun by an imaging system that resolves a few arcsec structures. Observations of solar polar region from an out-of-ecliptic view are new issues and a telescope to observe the structures near the polar region is required. A whole Sun imager of ~1 arcsec spatial sampling is proposed here. The whole Sun with extended corona can be covered by a 2D imaging device of 2K × 2K pixels at the distance of 1 AU from the Sun. An EUV imaging telescope like STEREO EUVI may be more

suitable than the X-ray telescope to observe polar plumes and inter-plume regions in polar coronal holes. In the late 2010's and early 2020's whole Sun EUV imagers are planned in Solar Orbiter and GOES spacecrafts and the presence of these imagers needs to be considered for the selection of the telescope bandpass. The SOLAR-C Plan-A EUV Activity Imager (Figure 18) is a Ritchey-Chretien telescope consisting of two hyperboloid mirrors. Each mirror is coated with Mo/Si multi-layers to enhance the reflectance of EUV light. The full width at half maximum of the reflectance as a function of wavelength is 10–15 Å around a central wavelength of each bandpass. Currently selected wavelength bands are 171, 195, 304, and 335 Å for their central wavelengths. A stereoscopic observation with SO will be possible at 171, 304, and 335 Å bands because the same EUV band with SO is selected. The CMOS APS is a primary candidate for the detector and the fall back plan is a back-illuminated CCD that was used in *Hinode*, STEREO, and SDO imagers. The imager on STEREO with a different selection of wavelength band can be a model payload.

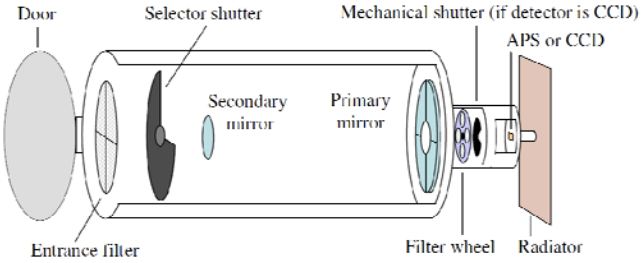

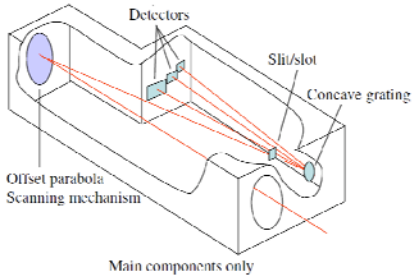

Figure 18. (left): SOLAR-C EUV Activity Imager
Figure 19. (right): SOLAR-C EUV Spectrometer

The imaging spectroscopy is a key instrument to detect the source of fast solar wind flows from polar coronal holes. The following performance is required: (1) the higher-throughput than SOHO SUMER and *Hinode* EIS for both quiet sun (QS) and active regions (AR), (2) 1 arcsec or slightly better spatial sampling, (3) a scanning rage of ±4 arcmin in the scanning direction, and (4) simultaneous observations of emission lines formed in the chromosphere, transition region, and corona. The SOLAR-C Plan-A science payloads have to be set at the side of the Sun, that is the spacecraft +Z direction, to the bus module because the surface of side bus panels located in the spacecraft ±X and ±Y directions are all used as radiators. Hence, the length of this imaging spectrometer must not be long like *Hinode* EIS, which is longer than 3.2 m in the Z direction. In order to realize a short instrument length without adding another reflection, the spectrometer needs to have a magnification using a single concave grating. The design of this type of spectrometer was first found by Roger Thomas (Thomas 2003). The instrument, SOLAR-C EUV Spectrometer (Figure 19), consists of a single off-axis parabola as a primary mirror of the telescope, a slit/slot selector, a toroidal (or ellipsoidal) concave grating with varied line space as a disperser, and solar-blind intensified CMOS detectors. Three wavelength bands are chosen to observe the chromosphere, transition region, and corona simultaneously: one is 310-340 Å (TBD), and 760-800 Å (TBD), and 1000-1100 Å (TBD).

The main body of these telescopes and imaging spectrometer are made of CFRP because of the weight reduction. In addition to the stringent contamination control of used materials including sufficient material bakeout, one point of note is that temperatures of all optical components should slightly be higher than that of the main body by the thermal design for a long-term stable instrument performance.

In the imaging spectroscopy with a grating spectrometer, there are two specific directions in the plane of the sky, that is, a slit direction and a scanning direction perpendicular to the slit direction. The direction along the slit will be in the north-south direction in the imaging spectrometer. It will be good to rotate the spacecraft around its Z axis for a specific observation to set the slit for any direction.

2.2.3 Solar Irradiance Monitor

The SOLAR-C total solar irradiance monitor is an absolute radiometer with cone-shape cavities. In front of each cavity there is a mechanical shutter to control the radiation input from the Sun. Each cavity has a heater and a thermal sensor, so that each can be a reference cavity. One of cavities is periodically exposed to the Sun. During the exposure, one of remaining cavities unexposed to the Sun is heated by the heater attached until the electrical heat input balances the solar input. For this operation there needs two cavities in this instrument at least. The cadence of periodic exposure is 1 min (TBD). There is degradation of the cavity surface by being exposing to the space environment, mainly due to solar UV illumination. To calibrate the degradation of the cavity surface, an infrequent exposure of a reference cavity to the Sun is needed. Probably, there will be another TSI instrument in low-Earth orbit at that time, so the SOLAR-C TSI monitor will also be calibrated to the other monitor when the SOLAR-C spacecraft is located in the ecliptic plane. There are a few groups to have heritage on developing the space TSI monitor, PMOD, JPL, LASP, and so on. A cross calibration to a cryogenic absolute radiometer is required before the flight.

2.2.4 Inner Heliospheric Imager (Optional)

A slightly-modified heliospheric imager on STEREO can be an optional candidate payload. The lens unit consisting of multiple optical lens has a large field of view (FOV) of about 60° and the FOV center to the Sun is offset by 45° around the spacecraft X-axis looking at space above the solar south pole when the spacecraft is in the ecliptic plane (Figure 20). When the spacecraft is located at the northern heliosphere, the heliospheric imager can look at the interplanetary space between the Sun and Earth. The spacecraft needs to rotate 180° around the spacecraft Z axis when the same interplanetary space is observed in the southern heliosphere.

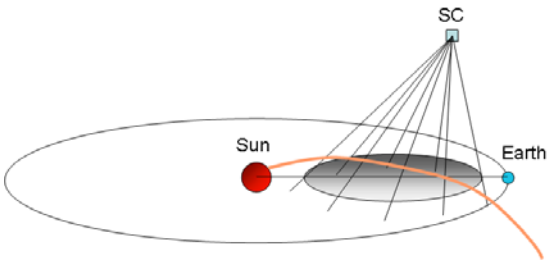

Figure 20. Field of View of Inner Heliospheric Imager

The scatted light level is reduced by the multiple baffles located in front of the wide-field lens unit. A 2D imaging device of 2K × 2K pixels that is cooled down to -60° is placed at the focal plane.

The brightest component is from planets in the solar system as a point source and the zodiacal light as diffused background. The bandpass is 5000-8000 Å (TBD) in the visible range. In order to avoid the blooming due to a bright object in FOV, a CMOS device will be preferable. Each image is obtained by ~1 min exposure duration. A multiple set of exposures is summed together by an on-board processing to enhance the component originating from electron scattering. The processed data are reformed into a telemetry data.

If the FOV of this instrument can point to the opposite side of the ecliptic plane by the spacecraft maneuver, a basic data set for determining the interplanetary dust distribution may be obtained for the first time.

2.2.5 In-Situ Instruments (Optional)

The role of in-situ instruments has not been discussed in detail in the SOLAR-C Plan-A working group. The out-of-ecliptic in-situ measurements were performed in the Ulysses mission. The orbit inclination is about 80°, which mostly covers the whole heliocentric latitude. The orbit is highly elliptical, so that the there is a period of a fast and a slow latitudinal scan for the heliosphere with different distances from the Sun. One major point of the SOLAR-C Plan-A orbit is that the spacecraft periodically travels between northern and southern maximum latitudes in a half year at nearly 1AU distance from the Sun. It is possible to do a research on the heliospheric physics that strongly depends on the solar cycle. A transport of cosmic rays in a solar cycle may become a target of SOLAR-C Plan-A regarding the production of cosmogenic isotope like ^{14}C and ^{10}Be, which are used as indices of the past long-term solar activity.

2.2.6 Other Instruments (Optional)

Since the SOLAR-C Plan-A spacecraft travels in a unique orbit, some instrumental proposals may arise from non-solar physics community. Although it may be important to consider them here to maximize a rare opportunity, it is beyond the scope of this proposal.

2.3 Spacecraft Requirements given from the Science Objectives

2.3.1 Attitude Control Requirements

On the SOLAR-C Plan-A there are imaging instruments that require periodic exposures in a long period of time, so that the spacecraft +Z axis is basically pointed to the Sun by a three-axis stabilized attitude control system (ACS). Since one of main payloads, which has marginally cover the whole Sun in the field of view, points to the Sun center for a day, a week, a month or a few months for the purpose of helioseismic and magnetic field observations, the nominal pointing direction is the center of the solar disk, so that the pointing coordinates of the other instruments with narrower field of view is restricted by the condition. Thus, when the other payload needs to look at a different location on the Sun outside its narrow field of view, the payload has to have a mechanism to change its own field of view. The tracking of the differential rotation of the Sun by the spacecraft attitude control is not required for observations with a small field of view.

Yohkoh and *Hinode* also have three-axis stabilized ACS and the spacecraft Y-axis is stabilized to point to the solar north. The functionality to rotate the spacecraft around the Z axis at any angle is to be requested, and provides a unique opportunity to observe scientific targets for the EUV scanning spectrometer that has a specific orientation in the plane of the sky. It is the slit direction. If the inner heliospheric imaging is adopted, the spacecraft rotation of 180° around the Z axis becomes mandatory and a step-by-step rotation of the spacecraft may sample the scattered photons from dusts in the solar system.

Table 5. Requirements for Attitude Control Stability (TBD)

Payload	Duration	ΔX, ΔY (arcsec)	ΔZ (arcsec)	Unit
- Imager - Spectrometer	1 sec	0.6		3σ
	10 sec	0.8		3σ
	5 min	1.6		0-p
	1 hr	*2.0	400	0-p
	24 hr			

*: will be better than *Hinode* due to no external disturbance except for solar radiation pressure in the interplanetary orbit. An exceptional period happens during the operation unloading the angular momentum of reaction wheels.

The spacecraft pointing stability achieved in *Hinode* completely satisfies the SOLAR-C Plan-A requirement. The long-term stability for an order of hour, a few arcsec per hour, will automatically be improved in SOLAR-C Plan-A, because the disturbance due to the thermal distortion disappears in the interplanetary space. Table 5 shows requirements for the attitude control system.

2.3.2 Time management

Except for the helioseismic instrument, the ISAS time tag system that was used in *Hinode* is applicable to SOLAR-C Plan-A. An additional requirement is given from the helioseismic instrument that requests a regular interval of exposure sequences. Table 6 summarizes the requirement for the time tag. The information of the time tag is distributed from the spacecraft data handling unit to the instrument controller of the helioseismic payload.

Table 6. Requirement of Spacecraft Time Tag (TBD)

Short term stability (1 – 100 sec)	± 0.5 ppm TBD	Requirement in SOHO
Long term stability (1 year)	± 1.0 ppm TBD	Requirement in SOHO
Duty cycle	0.5±0.05 sec	Requirement in SOHO

2.3.3 Data Compression and Data Storage

Since the telemetry should effectively be used, all the data need to be compressed on-board the spacecraft. The 12-bit lossless DPCM and lossy JPEG image compression were adopted in *Hinode* and a similar type of image compression is required in SOLAR-C Plan-A mission. It is efficient to compress the data in one box that is connected to all payloads, but the alternative is that each payload produces the compressed data to the spacecraft. The selection of the scheme is TBD.

The spacecraft is accessible from the Earth every day and the downlink will be periodically performed. But the total telemetry rate at the most distant location is not high and it is the bottle neck in the high-cadence observations. The following design philosophy will be applicable.

- Each payload can send the data to the spacecraft at any time.
- The data storage area is divided into small number of volume and each payload can send the data by a specified data storage volume.
- When the data are sent to the ground, one of data storage volume is dumped according to a planned schedule.

Some payload can do a high-cadence observation easily under this system, and the issue is the largest data size of a data storage volume that is related to the longest duration of the high-cadence of observation.

When the science data are produced in the rate of 100 kbps at the most distant part in the orbit during the science operation phase, total data volume per day is 8.2 Gbits (100 kbps × 1024 bit/kbit × 86400 s = 8.85×10^9 bits). However, the data rate can be higher when the distance to the spacecraft is shorter or when the Ka-band link condition is more stable than expected. When the 100 kbps data rate is possible at spacecraft position of 40° from the solar equatorial plane, the data rate can be 2.0 (3.3) times larger at 30° (25°). The capacity of the data recorder should be selected for an observing case of the maximum data rate condition. The tentative number may be 32 Gbits (TBD) including the spacecraft housekeeping data.

It will be useful from the operational point of view if the data recorder storage is divided into several independent volumes or partitions and if each payload can send the data by selecting one of volumes.

3 Spacecraft System

The spacecraft system design, including the orbit profiles and operation concept, are presented in this section. Section 3.1 summarizes the requirements to the spacecraft system derived from the discussion in the previous chapters. Obviously, the most important requirement of SOLAR-C Plan-A is to place the spacecraft at a high solar latitude. Working out the way to reach there dominates the mission design, which is discussed in Section 3.2. Several options are investigated, and an option using solar electric propulsion (SEP option) is presented as the primary option in this report. Based on the system requirements and the orbit design results, the spacecraft system for carrying out the mission is briefly investigated. The objective of the study is to confirm the feasibility of the mission mainly from the point of view of the resource budget, and its successful result is given in Section 3.3. The details of the subsystems are to be shown in Section 3.4, At this stage of interim report, however, the main focus is on those subsystems that require newly developed technology (communication system, light weight solar panel, and electric propulsion system), and the other subsystems are only briefly touched.

3.1 Spacecraft System Requirements

The major requirements to the spacecraft system (including orbit design) are,
- To reach the solar latitude of 40° by early 2020's.
- To support science instruments' mass of 130 kg (or larger).
- To transmit the scientific data continuously recorded in the rate of 100 kbps to the ground.

The third item is interpreted as the 300 kpbs down link rate under the assumption of 8 hours use of the ground station per day.

The following requirements are also recognized. However, they are regarded as non-dominating in the total system design and left for the further study in this report.
- Providing payloads a stable platform for imaging observations
- 150 W (TBD) payload power
- Regular notification of absolute time for regular-interval exposures required by the helioseismic instrument.

3.2 Orbit and Mission Profile

The SOLAR-C Plan-A is the first Japanese solar mission that operates in the interplanetary space. The following new issues in mission profile should be noticed when compared with the other Japanese (Earth orbiting) solar missions.
- It cruises in an interplanetary orbit, and takes much longer time to reach the final orbit.
- It only carries light payloads even if a heavy launcher (as H-IIA) is used.
- It is in severer radiation environments.

The following new issues from other Japanese interplanetary missions should be noticed as well.
- It requires much higher telemetry rate than ever achieved.

This item is not only reflected in the communication system design, but also considered in the orbit design to keep the distance from the Earth to the spacecraft short.

3.2.1 Trajectory Options for SOLAR-C Plan-A

The major mission requirement of SOLAR-C Plan-A is to observe the Sun from high latitudes. The target maximum latitude is tentatively specified as 40° (Figure 21a). To observe the Sun from the high latitudes, the space observatory (spacecraft) must be in an orbit largely inclined with respect to the ecliptic plane. It is not an easy task to inject the spacecraft into the orbit of this type. A rough estimate shows that the velocity increment required to inject the spacecraft into this largely inclined orbit is approximately 20 km/s (Figure 21b).

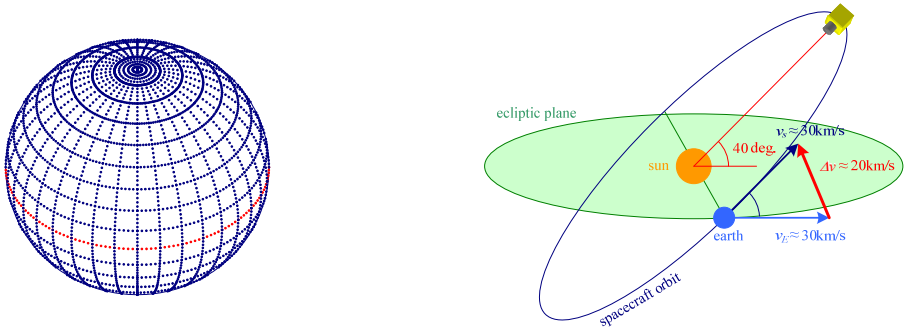

(a) View from lat. 40° of the sun (b) Challenge to lat. 40°

Figure 21. Schematics of Trajectory Design Challenge in SOLAR-C Plan-A

In order to achieve this severe mission target, possible trajectory sequences are investigated considering the application of various trajectory manipulation techniques. The items considered are, the geometric relation (i.e. the tilt of the solar equatorial plane to the ecliptic plane), launcher capacity, planetary gravity assists, and the usage of a highly efficient propulsion system. As a result, four major trajectory options are listed up to achieve the mission objective (Figure 22).

The first option is called “SEP option”, which is characterized by the usage of the solar electric propulsion (SEP) combined with the Earth gravity assists (EGAs). In this option, SEP is used to increase the relative velocity (v_∞) at the Earth encounter and the direction of $\mathbf{v}_\infty$ is changed by EGA to contribute to inclination increase. As a result of the sequential use of this process, latitude 40° can be achieved in five years from the launch. The other options are characterized by the usage of the planetary gravity assists only, without using SEP. The second option is called “Jupiter option”. In this option the operation sequence begins by using the Jupiter gravity assist (JGA) to highly incline the orbit plane from the ecliptic plane. What is unique to this option is the usage of EGAs in order to reduce the orbit period after JGA, which enables the frequent observation of the solar polar region. The remaining two options are characterized by the usage of EGAs and the Venus gravity assists (VGAs). In both options the operation sequence begins with the sequence of EGAs/VGAs to increase v_∞ to the planets. Then, the sequential planetary gravity assists are used to change the direction of $\mathbf{v}_\infty$ so as to contribute to incline the orbit. “Venus-1 Option” uses the Venus for the plane change gravity assists, whereas “Venus-2 Option” uses the Earth for this purpose.

Among the four options, the first “SEP option” has a major advantage in complying with the most of the mission requirements (the detail shown in 3.1.2). The option has frequent launch windows (every half year), which should be also counted as a merit from the programmatic point of view. On the other hand, it must be noted that this option requires an advanced technology, which is not required in the other options. This point will be discussed in 3.3. In view of the major advantage mentioned above, in the following part of Section 3, the case of SEP option is focused on. Alternative Jupiter option with the same final orbit is shown in Appendix B.

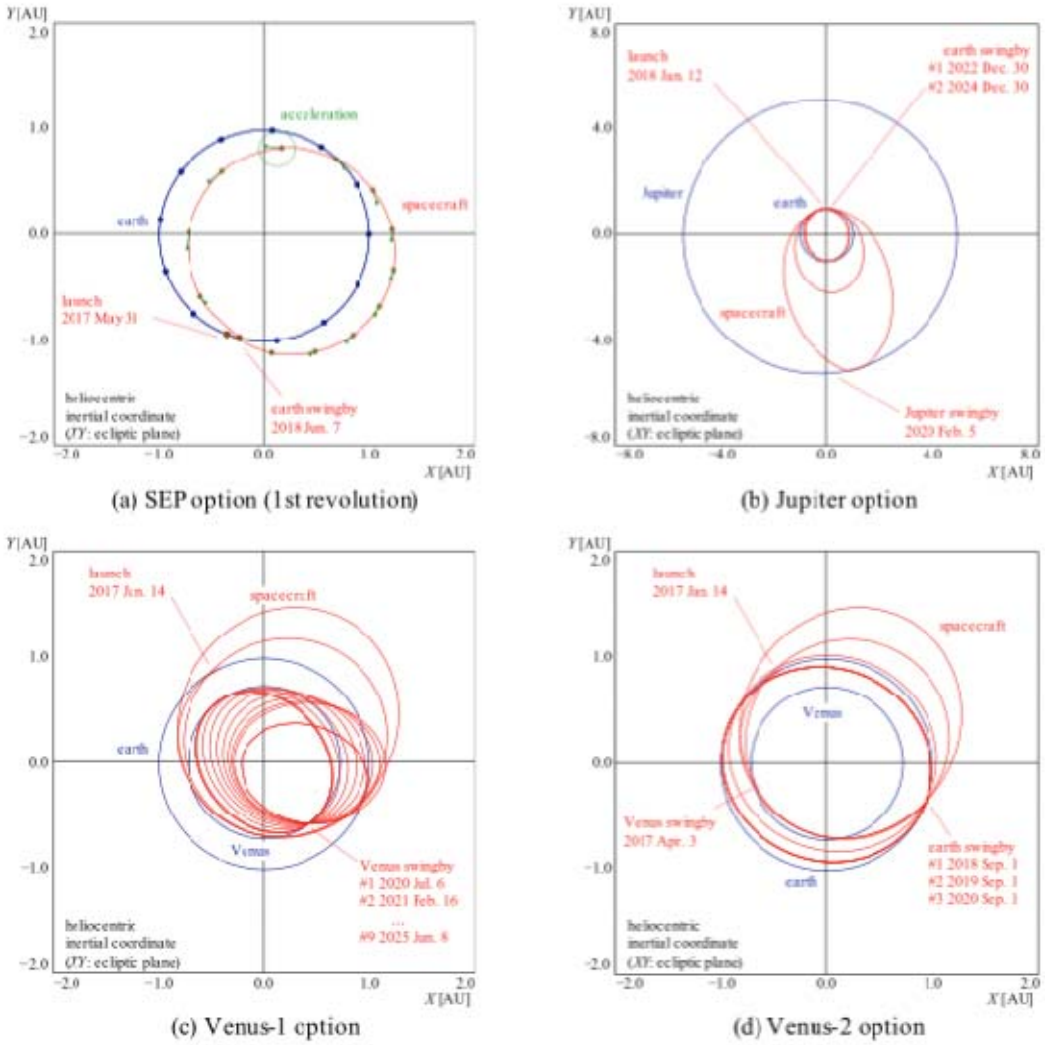

Figure 22. Trajectory Options for SOLAR-C Plan-A

3.2.2 Orbit and Mission Profile of SEP Option

Before showing the baseline sequence of the SEP option, a couple of its variants are introduced briefly. The first method, which is called “Direct Inclining Method (DIM)”, is a simple one which uses SEP directly to increase the inclination. The second method uses SEP combined with EGA, which is called Electric Propulsion Delta-V Earth Gravity Assist (EDVEGA). The method uses

EDVEGA repetitively, and is called “Sequential EDVEGA Method (SEM)”. Both methods were investigated quantitatively, and it was concluded that, DIM is infeasible from the points of view of the spacecraft’s mass budget and the operation time of the ion engine system (IES), whereas SEM is feasible in these aspects. A slight variation of SEM is also investigated, which applies an additional Venus gravity assist (VGA) prior to the sequential EDVEGA. This method has an advantage in reducing the launch energy drastically compared to the original SEM. However, the use of Venus/Earth gravity assists limits the launch opportunity, which makes it difficult to take advantage of the geometrical relation (i.e. the tilt of the solar equatorial plane to the ecliptic plane). From this point, the usage of VGA is regarded only as a backup option.

As a result of the discussion above, SEM is adopted and used to construct the baseline sequence of the SEP option. The basic procedure of SEM is described as follows.

1. The spacecraft is injected into the Earth synchronous orbit to re-encounter the Earth after one year cruise.
2. During the cruise, SEP is used to maximize the spacecraft’s relative velocity to the Earth (v_∞) at the next Earth encounter. Note that the thrust does not necessarily increase the inclination by itself. To enhance the efficiency to increase v_∞, an elliptic orbit is used for the cruise orbit.
3. By EGA, the direction of $\mathbf{v}_\infty$ is changed to contribute to the inclination increase.
4. By the repetitive use of the steps 2 and 3, the inclination is increased step by step.

Before presenting the constructed trajectory sequence, major assumptions used in the trajectory design should be noted.

The first assumption is related to the launch condition. The assumed launcher is the Japanese H-II A heavy launch vehicle equipped with a solid motor upper stage. The initial mass of the spacecraft is assumed to be 1200 kg. Assuming the practical settings of the launch site and the launch direction, the launcher is capable of injecting the spacecraft into the escape orbit with the excessive velocity (v_∞) of 7.3 km/s. The launch date is selected to take advantage of the not negligible tilt (7°.25) of the solar equatorial plane to the ecliptic plane, and they are June 7 or December 8. In the following discussions, June 7 is used as the launch date.

The second assumption is related to the ion engine system (IES). The specific impulse (Isp) of IES is assumed to be 3800 s, and the maximum thrust of IES is assumed to be 120mN in total. In the trajectory design, the actual thrust available for the maneuver is constrained by the available power, which is assumed to decrease as the inverse square of the distance from the Sun.

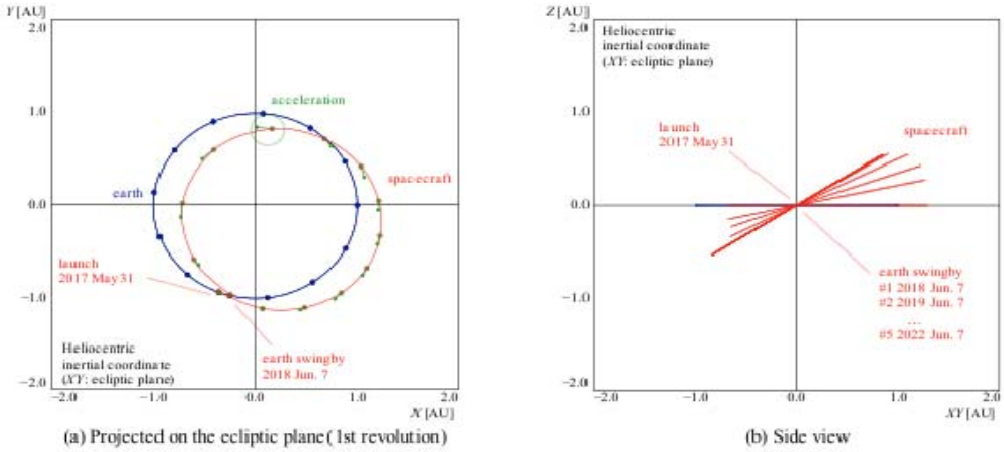

Figure 23. Trajectory profile of SEP option

The third assumption is related to the eccentricity (e) of the cruise orbit. To efficiently increase v_∞, the eccentricity e should be large. However, considering the difficulties in the thermal design of the spacecraft, the eccentricity e is constrained to be less than 0.3 in the trajectory design.

Figure 23 shows the trajectory profile of the SEP option. In Figure 23a, the trajectory of the first revolution is projected on the ecliptic plane. The figure shows that the spacecraft's orbit has eccentricity, and intersects with the ecliptic approximately at the Earth's position at the launch. The acceleration vectors indicate that the thrust is used to decelerate the spacecraft at aphelion and to accelerate the spacecraft at perihelion, which result in the increase of v_∞ at the next Earth encounter. Figure 23b shows the trajectory profile through the sequence. The trajectory is projected on the plane perpendicular to the ascending node direction so that the gradual change of the orbit plane can be easily seen. It is observed that the first four cycles have asymmetry resulted from the orbit eccentricity. However, the orbit is finally circularized by EGAs, which results in the symmetry observed in the final orbit (the orbit whose inclination is the highest).

Table 7. Sequence of events of SEP option

Date	Event	v_∞	i_{SEQ}
2017/05/31	Launch	7.3 km/s	7.2°
2018/06/07	EGA #1	9.8 km/s	7.3°
			18.8°
2019/06/07	EGA #2	12.3 km/s	20.2°
			25.8°
2020/06/07	EGA #3	14.6 km/s	27.2°
			33.0°
2021/06/07	EGA #4	15.7 km/s	34.9°
			38.1°
2022/06/07	EGA #5	16.6 km/s	39.8°
			40.0°

The sequence of events of the SEP option is summarized in Table 7. In the table, v_∞ denotes the relative velocity to the Earth at EGA, and i_{SEQ} denotes the inclination to the solar equatorial plane. The spacecraft reaches i_{SEQ} of 30° after the 3rd EGA (3 years from the launch), and finally reaches i_{SEQ} of 40° after the 5th EGA (5 years from the launch).

Figure 24 shows the profiles of some important parameters of the mission. The top chart indicates the points of events and basic operation concept. The following three charts respectively show the profile of the spacecraft's distance from the Sun and the Earth, its instantaneous solar latitude, and the expected down link rate of the scientific data.

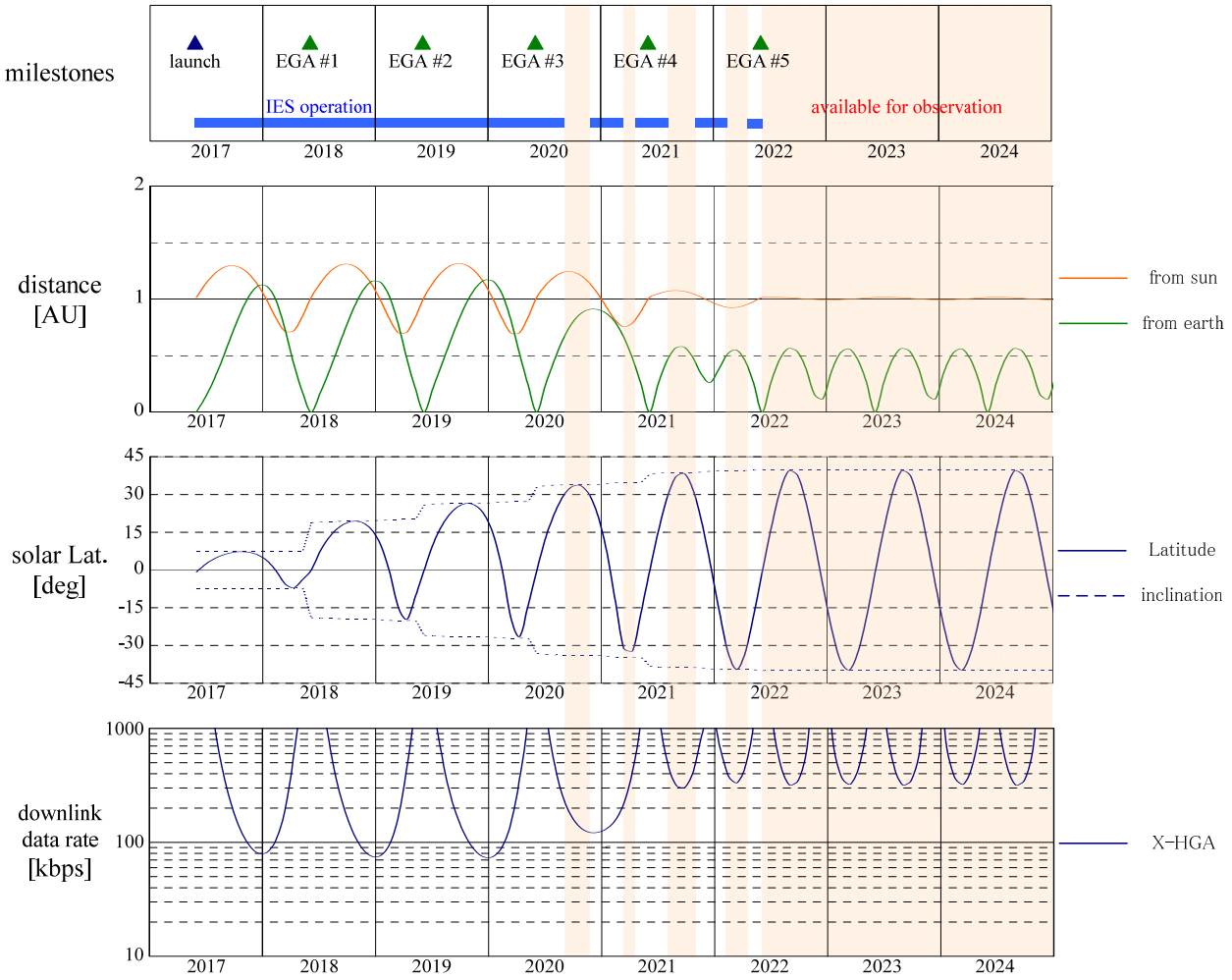

Figure 24. Mission profile of SEP option

In the first three years from the launch, before the spacecraft reaches i_{SEQ} of 30°, the spacecraft operation is devoted to increase the inclination. IES is operating most of the time, and silent condition for the scientific observation is basically not guaranteed in this phase. Even in this phase, intermittent suspension of IES is planned for accurate orbit determination, which may be used as

occasions for observations. In the fourth year, after EGA #3, i_{SEQ} exceeds 30°. From this year onwards, the period during which the spacecraft is at latitudes higher than 30° is allocated as "the observation phase (orange area in Figure 24)", and the IES operation is intentionally suspended. Even after EGA #3, IES operation is continued while the spacecraft is in the lower solar latitude. This IES operation and the following two EGAs contribute to the further increase of the inclination and the circularization of the orbit. Finally, as a result of EGA #5, the spacecraft is injected in to the final observing orbit, the circular one-year orbit with i_{SEQ} of 40°.

3.3 Spacecraft System Design

The SOLAR-C Plan-A is the first Japanese solar mission that operates in the interplanetary space. The following new issues in spacecraft system design should be noticed when compared with the other Japanese (Earth orbiting) solar missions (a part of issues results from the mission design).
- It requires a much longer mission life.
- It is in severer radiation environments.
- It carries light payloads only.
- It requires large solar array panels
- It requires fuel to keep three-axis attitude control.

The following new issue from other Japanese interplanetary missions should be noticed as well.
- It requires much higher telemetry rate than ever achieved.

This item is already considered in the orbit design, and is also reflected on the communication system design. In addition, it should be noted that, as a result of using a liquid fuel rocket (H-IIA), the mechanical environment at the launch is relaxed from that in case of using solid rocket as previous solar missions.

3.3.1 Spacecraft Configuration

The mission design provides basic information of the spacecraft configuration. The required thrust determines the configuration of IES, and the configuration of IES determines the required power which finally determines the size of solar array panels (SAP). The orbit design provides the geometrical relation around the spacecraft during the mission, which determines the basic location of the key components. As a result, the basic configuration the spacecraft is determined as shown in Figure 25.

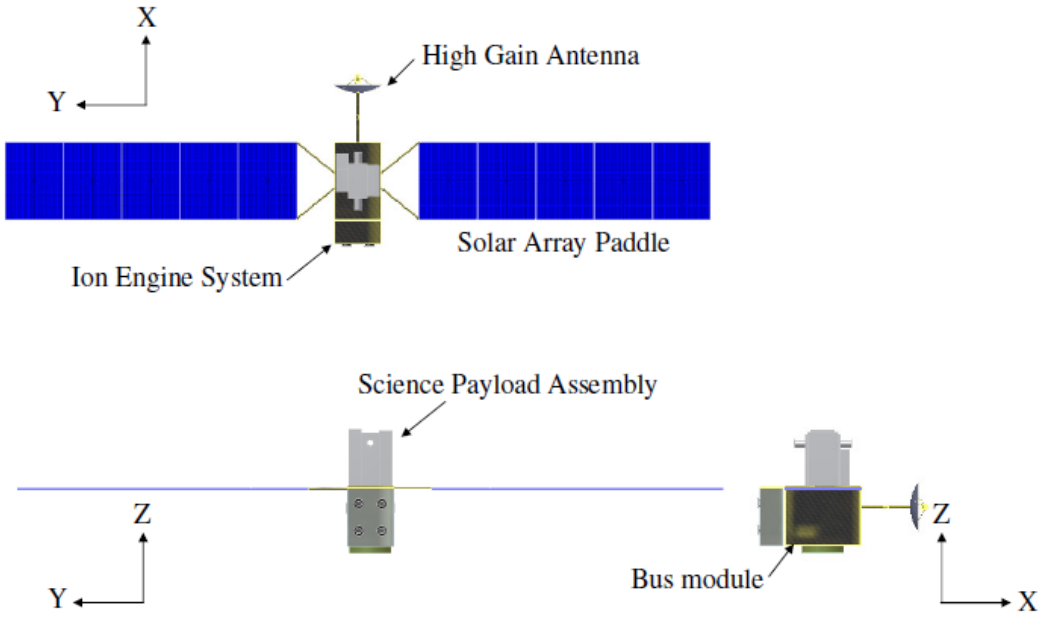

Figure 25. Spacecraft configuration of SEP option

The spacecraft's +*Z*-direction is always pointing to the Sun. The scientific payload assembly is mounted on the +*Z* panel of the bus module and pointing to the Sun. SAP are deployed from the bus module to the ±*Y*-direction and fixed to the body, facing the +*Z*-direction. In the trajectory design process, IES thrust direction is constrained to be approximately normal to the Sun direction, which enables IES module to be mounted on the –*X* panel. The panels not facing to the Sun direction (±*Y*, –*X*, -*Z*) are used as radiator panels to dissipate the large heat generated by IES components. The geometrical relation among the spacecraft, the Sun and the Earth varies as a function of time. Therefore, a high-gain antenna for the high rate data transmission must be maneuverable, and mounted on the +*X*-panel.

3.3.2 Mass Budget

In order to confirm the feasibility of the mission, the spacecraft mass budget is estimated. In the investigation, the total mass of the spacecraft is assumed to be 1,200 kg (which complies with the assumption of the trajectory design), and the difference with the sum of subsystem masses is counted as margin.

For most of the subsystems, the composition of the components is considered, and the mass of components is summed up to the subsystem mass, while the mass of subsystems such as structure, harness, etc. is estimated parametrically based on the previous spacecrafts. The propellant mass for IES is derived from the trajectory design result.

The resulting mass budget is summarized in Table 8. The positive margin of 106 kg indicates the feasibility of the mission from the point of the spacecraft's mass budget.

Table 8. Spacecraft mass budget of SEP option

Item			Mass (kg)
Total mass			1200.0
	Dry mass		828.4
		Mission payloads	130.0
		Data handling system	6.7
		Communication system	94.6
		Power supply system	84.1
		Attitude control system	79.9
		Chemical propulsion system	36.5
		Ion engine system	161.9
		Structure / mechanical Int.	166.9
		Thermal control system / Thermal Int.	14.8
		Electric Int.	53.0
	Propellant		265.9
		for chemical propulsion	30.0
		for ion engine system	235.9
	Margin		105.7

3.3.3 Power Budget

In order to estimate the size and mass of SAP, the required power for the spacecraft is estimated. In the investigation, two cases of power budget (IES operating / non-operating) are estimated. The composition of the components is considered, and the powers for the components are summed up to the subsystem power. The resulting power budget is summarized in Table 9.

Table 9. Spacecraft power budget of SEP option
(Heater powers for payload not included.)

Item		Power (W)	
		IES op.	IES non op.
Total power		6065.7	1553.6
	Mission payloads	0.0	150.0
	Data handling system	12.3	12.3
	Communication system	128.8	128.8
	Power supply system	97.7	97.7
	Attitude control system	165.0	165.0
	Ion engine system	5637.0	0.0
	Thermal control system	24.9	999.8

The mass of SAP is estimated on the basis of supplying the power for IES operating case at 1 AU. The use of newly developed light weight SAP is assumed, and the specific value of 100W/kg is

used in the estimation. The resulting mass of SAP is included in the power supply system in the mass budget.

3.3.4 Communication Link Budget

In order to confirm the feasibility of the high rate data link, the communication link budget is estimated under the assumed communication system configuration. In the investigation, two cases of link budget (X-band / Ka-band) are estimated. The maximum distance of 0.56 AU in the final orbit is used, and NASA/DSN 34m antenna is assumed as the ground station. The resulting link budget is summarized in Table 10.

Table 10. Communication link budget of SEP option

Item	X-band	Ka-band	unit
Frequency	8400	32300	MHz
Transmitter power	40.0	20.0	W
Transmit antenna gain	36.5	48.2	dBi
Communication distance	0.56	0.56	AU
Data rate	300k	1M	bps
Link margin	1.0	2.0	dB
Received C/N0	59.3	64.6	dBHz
Required C/N0	58.4	62.6	dBHz

The positive margin of 1 dB for 300 kbps downlink indicates the feasibility of satisfying the system requirement in the final orbit. It should be noted that this downlink rate is achieved by more reliable X-band link. In addition, 1 Mbps downlink by Ka-band link is expected with positive margin of 2 dB.

3.3.5 System Thermal Design

In the cruise phase of SEP option, the minimum solar distance (i.e. perihelion distance) is to be 0.7 AU. It is assumed that three μ20 ion engines are simultaneously used even at the perihelion passage. The amount of heat dissipated from IES is estimated to be approximately 1,800 W in total, and it is not easy to radiate this amount of heat to space. In order to confirm the feasibility of the thermal design, system thermal analysis is conducted. In the analysis, the simultaneous use of the three μ20 ion engines at 0.7 AU is assumed as the worst case. The Sun-light is assumed to input from the direction 5° apart from $+Z$ direction, which causes the heat input from the Sun into the side panels of spacecraft.

The thermal mathematical model consisting of the spacecraft bus module and ion engine module is constructed, and a steady state thermal analysis is conducted. The result shows that we can still

have a feasible solution under this worst condition. The solution requires that concentrated heat dissipation from the ion-engine related components to be averaged at each structure panel by heat pipes and thermal doublers.

3.4 Spacecraft Subsystems

The spacecraft subsystems are discussed in this section. At this stage of the interim report, the investigation gives priority to the subsystems that require new key technologies to achieve this mission. They are Ka/X communication system, ultra-lightweight solar panels, and μ20 ion engine system. The details of these subsystems are given in Sections 3.4.2, 3.4.3 and 3.4.6 respectively. As for the other subsystems, the functions required to them are supposed to be achieved with proven technologies. Their compositions are tentatively assumed based on the previous missions, and they are only briefly touched in this report.

3.4.1 Data Handling System

The data handling subsystem are supposed to be composed based on the heritage of the previous interplanetary spacecrafts, *Hayabusa* or *Akatsuki*. It is composed of DHU (data handling unit) and TCIM (telemetry command interface module). DHU manages the automatic/autonomous function of the spacecraft bus system, collects and records the HK (house keeping) data, and manages DH network as the host. TCIM interfaces telemetry and command between DHU and the communication system. It generates the transfer frame and multiplexes the telemetry packets, and output to the transmitter. On the other hand, it modulates the uplink signal input from responder, and output command packets to DHU.

3.4.2 Communication System

Since the spacecraft is in the interplanetary space for the out-of-ecliptic mission, a high-speed telemetry is mandatory for imaging observations of the Sun. We have tentatively set a straw-man data recording rate of 100 kbps in X-band considering the continuous helioseismic observations. This level has been achieved in the NASA STEREO mission in the distance of 0.5 AU from the Earth. On the other hand, the Japanese interplanetary missions that have so far been flown only achieved the telemetry rate of less than 10 kbps using 64m-aperture downlink station at Usuda deep space center. When the downlink duration is limited to 8 hours per day for example, 300 kbps telemetry rate is required for 100 kbps recording rate. If this should be achieved by a domestic effort, a development of a high-power transponder will be required in addition to reducing any transmission losses.

Based on the consideration above, the following design guideline is derived.
- Achieve 300 kpbs downlink rate assuming the downlink duration of 8 hours per day.
- Use X-band system heritage in interplanetary communication for stable and assured downlink.
- Use Ka-band system for a higher-telemetry capability under good atmospheric conditions.

- Adopt domestic supplied components which we can have by around year 2012.
- Adopt a high gain antenna of 1.6 m diameter.
- Adopt a high-power (40W) X-band transmitter as a natural extension from the JAXA heritage.
- Reduce feeder loss compared with the previous JAXA interplanetary missions.
- Improve the coding gain by the modification of coding method.

The block diagram of the communication system (with the heritages) is shown in Figure 26.

In order to have a higher data transmission rate or a shorter downlink duration, the use of Ka-band system is supposed in addition to the X-band system. The downlink of Ka-band telemetry is possible at the NASA DSN stations to track the STEREO spacecrafts. Since the availability of Ka-band is affected by the atmospheric condition on the Earth, the Ka-band alone cannot be a solution to the requirement set by the continuous helioseismic observations.

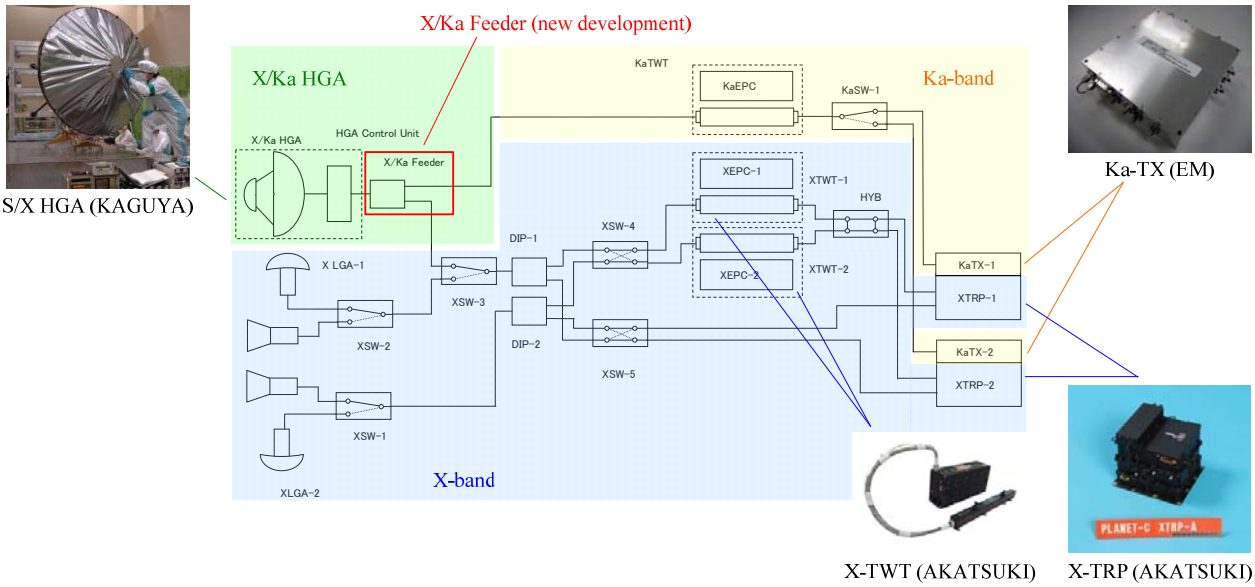

Figure 26. SOLAR-C Communication System

3.4.3 Power Supply System

Power supply system of SOLAR-C Plan-A consists of Power Control Unit (PCU), Series Switching Regulator (SSR), Solar Array Paddle (SAP), Battery (BAT), and Pyrotechnic Controller (PYC). In the system, the output voltage of SAP is lowered and stabilized by SSR. The functions of PCU are SSR control, BAT charge/discharge control and management, and the bus power distribution. BAT is used for power supply when SAP cannot supply sufficient power. The cases supposed are, the launch phase, the attitude anomaly, and the large attitude maneuver. The use of Lithium ion battery is supposed based on the heritage of the previous interplanetary spacecrafts, *Hayabusa* or *Akatsuki*.

SOLAR-C Plan-A spacecraft is propelled by the ion engine system. In order to operate three μ20 ion engines simultaneously, approximately 6 kW of power is required to be supplied by SAP. When conventional rigid type SAP is adopted, its mass is estimated to exceed 100 kg. On the other

hand, the reduction of components' mass is strongly requested as a general nature of interplanetary spacecraft. From this consideration, the newly developed ultra-lightweight solar panel is used to meet the requirements of high specific power (W/kg) and low storage volume. This component is identified as the key technologies to achieve this mission.

The ultra-lightweight solar panel is now under development in ARD/JAXA, and uses newly developed space solar sheet supported by a frame-type structure (Figure 27). It is targeting the specific power greater than 100W/kg in panel level. Future perspective of the ultra-light weight solar panel development is shown in Figure 28. Breadboard model was developed last year, and a series of development tests (vibration, thermal vacuum, and deployment test) were successfully conducted. The technical readiness level (TRL) is estimated to be 6+α.

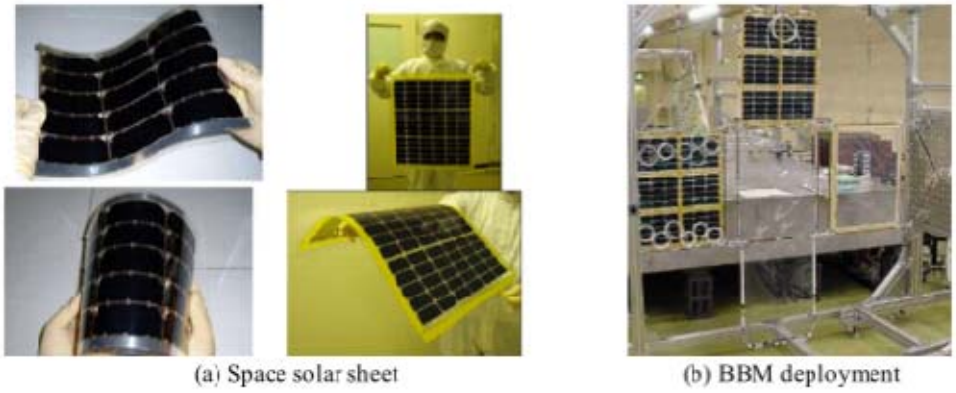

Figure 27. Ultra-Lightweight Solar Panel

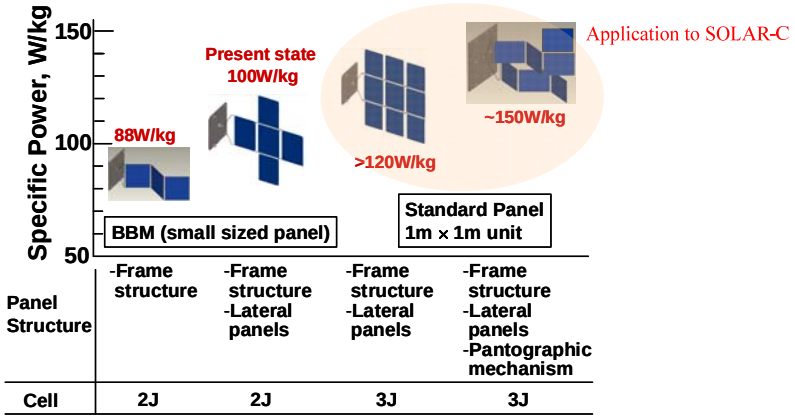

Figure 28. Future Prospects of Ultra-Lightweight Solar Panel Development

As mentioned in Section 3.3.1, in the configuration of this spacecraft, Z-axis (the direction perpendicular to SAP) is basically pointed toward the Sun. Therefore, SAP is fixed to the spacecraft body, and no driving mechanisms are installed.

Li-ion battery is adopted as a high-density power cell in the Plan-A spacecraft. The overcharge and over-discharge protections are dealt by the Series Switching Regulator (SSR) that has been developed in the JAXA MMO mission. The bus voltage regulation is made by SSR monitoring the electric current at BAT. The period in which the spacecraft is operated by the power from BAT is

(1) during initial phase just after launch, (2) during orbit control without using the ion-engine system, and (3) during the safety state in an attitude control for emergency cases. The eclipse period in which the Sun cannot be seen does not happen in the SOLAR-C Plan-A orbit except for the launch operation. The capacity of battery is selected by these conditions and it is found to be about 27 Ah (TBC) in the first estimate.

3.4.4 Attitude Control System

The requirements for the attitude control are summarized in Table 5. The three-axis stabilization is required for imaging observations of an arcsec spatial resolution. The attitude control system that is tentatively assumed here is what was used in *Hinode* mission. Since the short-term performance of the *Hinode* attitude control system completely satisfies the SOLAR-C Plan-A requirements, no improvement is necessary. The external disturbance in the interplanetary space is much smaller and more stable than that in the low-Earth orbit, so that the main source of disturbance is the mechanical motions within the spacecraft. One of the differences between SOLAR-C Plan-A and the Japanese solar missions in low-Earth orbits is the use of chemical thrusters to unload the angular momentum accumulated in the reaction wheels (RW). According to a simple calculation, the frequency of the RW unloading is estimated to be once per day in a nominal science operation. The helioseismic instrument may need to have its own image stabilization tip-tilt mirror to compensate the long-term pointing change or to stabilize the unexpected low-frequency disturbance.

3.4.5 Chemical Propulsion System

Chemical propulsion subsystem is used for unloading of the RW accumulated angular momentum and the attitude maneuver which requires large control torque (such as initial attitude establishment and safe hold mode operation). The thrusters are also used for the short term translational motion control such as the trajectory correction before the Earth gravity assists. Considering the level of the total impulse required, the conventional monopropellant (N_2H_4) system is assumed at the present phase.

3.4.6 Ion Engine System

Owing to the success of Japanese asteroid explorer HAYABUSA, which has an ion-engine μ10 system for interplanetary cruise, ISAS/JAXA has a heritage of ion engines. ISAS is developing the scale-up version of the ion engine thruster, μ20. Figure 29 shows the engineering-model thruster, which is in an endurance running test under a vacuum condition. We assume a SEP system in which four sets of ion engines are set on the spacecraft and three out of four can be turned on simultaneously. In the orbit design we assume the thrust of 40 mN and specific impulse of 3,800 s for each thruster or the maximum thrust of 120 mN for simultaneous use of three thrusters.

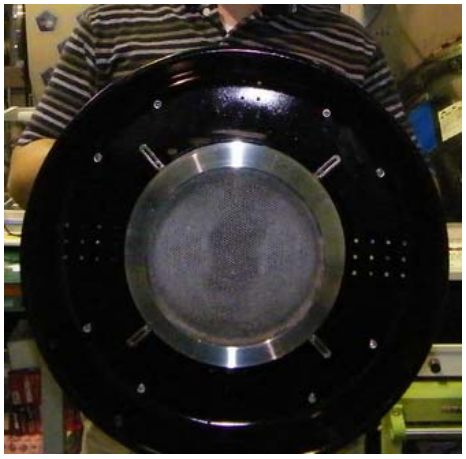

Figure 29. Engineering model of μ20 ion engine thruster

The μ20 ion engine system consists of Ion Thruster Control Unit (ITCU), IES Power Unit (IPU), Propellant Management Unit (PMU), Ion Thruster Assembly (ITA), Microwave Supply Unit (MSU), and IES Pointing Mechanism (IPM). Xe is the propellant of this engine. Xe ions are produced in a process of discharge by microwaves and are accelerated by electric fields between two grids. The role of each unit is summarized as follows:

IPM: This is a pointing mechanism of ITA.
IPU: This produces a high voltage (~2.3 kV) to accelerate Xe ions.
ITA: This unit produces thrust from Xe propellant, microwaves, and high-voltage applied.
ITCU: This unit controls the whole ion-engine system (IES).
MSU: This unit supplies microwaves to ionize Xe for acceleration and to make electrons for neutralization.
PMU: This unit provides Xe propellant to ITA.

Each ion engine thruster produces the thrust of 40 mN. By simultaneous use of three μ20 ion engines, one of which is currently being developed and tested at ISAS, the maximum thrust of 120 mN is obtained. Some components are set on the spacecraft bus structure, and some are set on the Ion Engine Module (IEM) that is an independent box located outside the spacecraft bus structure. IEM has six ion engine thrusters, two of which are redundant engines for unexpected situations. The IPM connects IEM with the spacecraft, and it also acts as a pointing mechanism that slightly tilts the whole IEM to control the direction of thrust under combinations of multiple ion engine thrusters, each has a slightly different thrust and is located at a different distance from the center of gravity of the spacecraft.

Power Control Unit (PCU) on the spacecraft provides the power of 350 W (1,520 W) with MSU (IPU) for operating each ion engine thruster. 1,870 W electric power is required for operating a single ion engine thruster. It was 350 W for *Hayabusa*'s μ10 ion engine system. Larger power consumption in the SOLAR-C Plan-A system gives large heat generation that needs to be radiated away from the spacecraft. The ion engine system in the Plan-A spacecraft produces a huge amount of heat that cannot be radiated away from the surface of IEM alone. In order to have a solution for

the heat dissipation problem, some components, ITA and MSU, are set in IEM, and other components, ITCU, IPU, and PMU, are mounted in the spacecraft bus structure.

In the following points the system is different from *Hayabusa*'s ion-engine system. These are all related to the increase in weight or heat dissipation to achieve high thrust in good propellant efficiency.

1. Size of ITA from 10 cm diameter in *Hayabusa* to 20 cm diameter in SOLAR-C Plan-A
2. Operating power for ion acceleration
3. Pointing mechanism at IPM

Currently estimated specifications summarized in Table 11 assume higher specific impulse options that will soon be applied to the EM thruster under endurance test. Original test conditions of the EM thruster's ion source were 1,300 V (Screen Voltage), 30 mN (Thrust) and 2,800 sec (Specific Impulse), respectively, and it accumulated 10,000 hours of operation by Sep. 2010. The technical readiness level (TRL) is estimated to be 4-5.

Table 11. SOLAR-C Plan-A Ion Engine System

Propellant	Xe	
Specific impulse	3800 s	
Thrust	40 mN/engine	
Screen Voltage	2300 V	
Number of thrusters	4	
Maximum number of thrusters that run simultaneously	3	
Size of Ion-Engine Module	1,200×1,500×600 mm	
Pointing mechanism	Newly proposed linear actuators Range: ±5°	Need a development
Weight	162 kg	Estimate in 2010
Weight of Fuel (Xe)	236 kg	Estimate in 2010
Power	5,650 W Regulated bus: 1,090 W Non-regulated bus: 4,560 W	Estimate in 2010

3.4.7 Structure System

A box-type panel structure is adopted as the spacecraft main body (bus module). The approximate size of the main body is 2m×1.2m×1.5m. The scientific payload assembly is mounted on the $+Z$ panel of the bus module, and the rocket attachment ring is installed on the $-Z$ panel. The movable IES module is installed on the $-X$ panel. Two axes pointing mechanism enables to direct the IES thrust axis to the spacecraft center of mass. The major deployable appendages are two wings of

solar array panels and Ka/X-band high gain antenna. The solar array panels are installed on the ±*Y* panels, and they are latched and fixed to the body after deployment. Two axes gimbaled movable high gain antenna is installed on the +*X* panel, and is deployed after the launch.

3.4.8 Thermal Control System

SOLAR-C Plan-A spacecraft is propelled by the ion engine system. When three μ20 ion engines are simultaneously operated, the heat dissipated from IES is estimated as approximately 1,800W in total. The major theme for the thermal control system is to radiate this large amount of heat to space. In order to achieve this objective, large areas on the structure panels that are not facing with the Sun (±*Y*, –*X*, -*Z*) are used as radiator panels. Concentrated heat dissipation from IES is transferred and averaged at each structure panel by heat pipes and thermal doublers. The area outside the radiators on the structure panels is covered with the multi layer insulator (MLI), to interrupt unnecessary heat input/output.

When not all the ion engines are operated, the reduced heat dissipation from IES is compensated by heaters. The heater control electronics (HCE) automatically controls the duty of the heaters based on their priority. It enables the appropriate management of the power allocation between thermal control and IES operation even when the available power is limited around the aphelion.

Appendix

Appendix A:

A.1 Exploration of α-effect and turbulent diffusion

While it is generally accepted that differential rotation is the main player transforming poloidal into toroidal field the details of the processes rebuilding the poloidal field from toroidal field are still uncertain. In the mean-field language these processes are formally described as α-effect. In the near surface layers it is in principle possible to observationally constrain the amplitude of turbulent flux dispersal from models that describe the surface evolution of magnetic field.

In the context of solar dynamo models the following mechanisms for the α-effect are generally considered: 1. Helical turbulence, 2. MHD shear flow instabilities in the tachocline, 3. Rising flux tubes in the convection zone influenced by Coriolis force and convection (Babcock-Leighton). While all these processes are likely to contribute, their amplitude and spatial distribution is not known well enough to clearly quantify their individual role. Furthermore, recent research points toward a highly non-linear and also time dependent α-effect resulting from additional constraints due to conservation of magnetic helicity.

In general it is not possible to verify or rule out α-effect mechanisms within the convection zone through photospheric observations. However, some insight into the poloidal field generation mechanism might be possible. In particular measurements of the transport of magnetic flux in the polar regions by super-granular flows and meridional circulations will provide insight into efficiency of the Babcock-Leighton mechanism. Note that there is a strong correlation between the way the surface Babcock-Leighton term is modeled and quenched (in 2-D mean field models) and the resulting amplitude of the poloidal field near the poles. Precise observations of the timing, structure and strength of the poloidal field is thus key to constrain this fundamental ingredient in solar dynamo models.

A.2 Flows associated with flux emergence

An integral part of the current paradigm is the flux emergence process which consists of the buoyant rise of strong field from the base of the convection zone toward the solar surface and ultimately the formation of active regions.

Direct observations to confirm or disprove this picture are still rare but are of fundamental importance and need to be improved systematically with SOLAR-C In addition to jet like flows of a few 100 m/s that might be present at the base of the convection zone, a rising flux tube in the convective envelope induces additional motions with speeds in excess of 100 m/s based on thin-tube simulations as well as more recent 3D simulations. This flow is a superposition of the emerging upward motion and the downdraft due to the gravity and has slightly asymmetric structure in the east-west directions. A flux tube is expected to spend most of the time (about 1 month) in the lower part of the convection zone and only a few days in the upper most 20 Mm.

However, the rise speed in the near surface layers can reach values of about 1 km/s and is therefore more likely detectable.

Helioseismic signatures of sunspots have a large contribution from the near surface regions, where the relative perturbations of wave speeds are maximal. Our ability to seismically image the subsurface structure of sunspots depends strongly on a good understanding of near surface effects. The primary source of near surface thermal perturbations is caused by the Wilson depression. Independent measurements of this contribution in the near surface layers allows us to refine helioseismic tools and improve their focus on magnetic perturbations in the deeper layers. The second vantage point of a high latitude mission would allow for stereoscopic measurements of the Wilson depression, provided the imaging quality of the telescope is sufficient to resolve umbral dot like features in a sunspot umbra.

Helical turbulence generates helical mean fields. Since magnetic helicity is conserved in highly conductive fluids, small-scale magnetic helicity of the opposite sign must be shed through the photosphere or dissipated through Ohmic diffusion in order to sustain the large-scale dynamo. Evidence for helical field topologies or small-scale magnetic helicity flux through the photosphere might therefore be construed as an observational signature of the turbulent α-effect.

Vector magnetograms will also help quantify the global distribution and flux of magnetic helicity in and through the photosphere which has profound implications for the operation of the turbulent dynamo (Section3.3). High-latitude magnetograms will also enable a more thorough evaluation of the effects of surface magnetism on global oscillation frequencies, potentially improving the sensitivity of global rotational inversions. This is crucial for detecting the subtle signatures of zonal flows possibly associated with subsurface toroidal magnetic flux. In addition, observations of polar magnetism and related emission on the Sun will help interpret stellar observations by calibrating proxies used to infer magnetic activity.

Magnetic helicity is thought to play a key role on the operation of small versus large scale dynamo in the Sun. It can be demonstrated that for fast processes with respect to magnetic diffusion and by defining a reference magnetic field, a gauge invariant magnetic helicity can be defined in diffusive open system such as the Sun. It is also well known that stability conditions of the surface magnetic structures are dependent on their magnetic helicity budget and the injection of magnetic flux and helicity by the convection. This quantity can thus serve a very important role since it can relate inner and outer magnetism helping us to draw and improve our theoretical view of the solar magnetism in a more integrated way.

While it is in principle possible to detect helical flows in the convection zone or nonaxisymmetric flows resulting from MHD instabilities in the tachocline, it is not clear how to relate these flows to an α-effect without making very strong assumptions (first order smoothing, second order correlation approximation), which cannot be justified for the solar parameter range from first principles. In that sense a measurement of these flows can be taken only as an indication for a potential α-effect in these regions. On the other hand the contribution from the Babcock-Leighton α-effect can be constrained by observations of the flux-budget in the photosphere. Pure Babcock-Leighton flux-transport dynamo models typically lead to a polar (mean) field strength of about 100 Gauss (if solutions are normalized to about 10^4 Gauss at the base of the convection zone) clearly in excess of the observational constraints around 10 Gauss. The latter shows that likely additional α-effects within the convection zone or tachocline exist and it has been shown that their inclusion

leads to models consistent with surface observations. A detailed study of the surface flux budget at all latitudes will promote a better understanding of the mechanisms of poloidal field regeneration in the sun. In particular, a quantitative determination of the contribution from Babcock-Leighton sources will impose additional constraints on (unobservable) sources within the convection zone and tachocline. Meanwhile, observations of magnetic helicity may be used to help assess the role of the turbulent α−effect (Section 3.3).

A.3 The inclination requirement

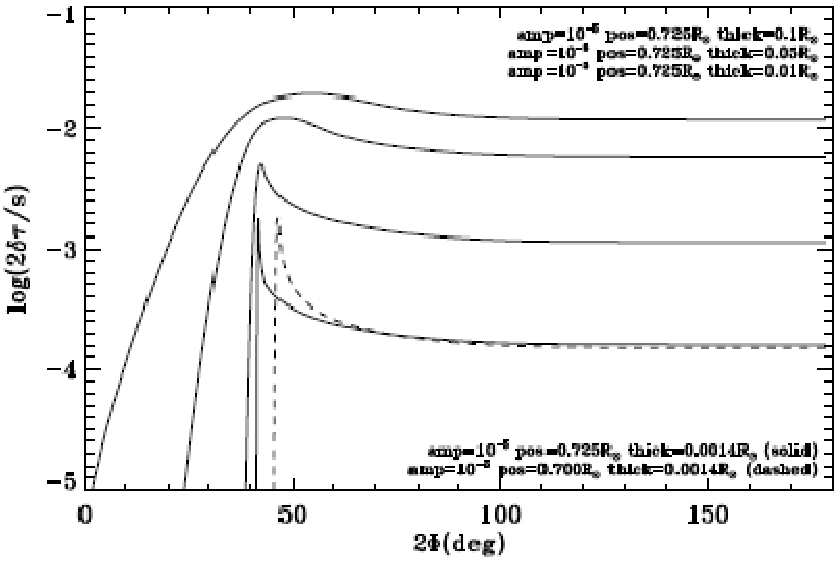

Figure 30. Travel-time perturbation $2\delta\tau$ computed for various combination of position and thickness of soundspeed perturbation of the size 10^{-5}, against full skip angle 2Φ.

We have so far established that observing the sun from a high-inclination orbit may well be desirable in our attempt to study dynamical processes in the solar interior and ultimately understand the solar dynamo. The advantage we will have, however, would not be by orders of magnitude in terms of our primary observables such as, say, travel-time measurement, because projection effect is just a matter of a factor except near the very edge, where Doppler signal would be dominated by horizontal motion brought about by convection. Let us look at an example.

According to the ray theory, a ray that reaches tachocline, around r/R_{sun}~0.7 has a skip angle of ~45°. If one is aiming at observing tachocline at the solar equator and immediately beneath the disc centre, the product of two foreshortening factors, by which we lose special resolution and the vertical component of velocity, is only $\cos^2(22.5°) \sim 0.85$. It is generally believed, however, that at least some of the key dynamical features are at higher latitudes. For a ray that begins at 7.5° latitude, travels down to tachocline at 30° latitude and returns to the surface at latitude 52.5°, during all which staying within the meridian, the product is $\cos(7.5°)\cos^2(52.5°) \sim 0.6$. For a feature at higher latitudes, the figure will be worse but, it is clear that we are talking only about improvement by a factor 2 or 3. We would like to point out, however, that even a factor of 2 may turn out to be crucial at the end of the line of our investigation into the deep interior.

More complete analysis of detection capability for a certain signature in the solar interior, by time-distance helioseismology, should take the following steps.

1. Travel-time perturbation: calculate the magnitude of travel-time perturbation for a given pair of points on the solar surface for which cross-correlation function is computed. This can be done by a simple ray approximation, by a more sophisticated method such as Born approximation, or by direct numerical simulation of wave propagation.

An example-- travel-time perturbation due to sound speed anomaly near the base of the solar convection zone (Figure 30). Perturbation to travel time 2τ (here τ is the travel time from the surface to the inner turning points) has been computed for the relative sound speed perturbation $\Delta c/c = 10^{-5}$, and various position and thickness, by ray approximation. The ray path Γ is determined by local group velocity $d\omega/dk$ of pure acoustic waves for which local dispersion relation $\omega=kc$ holds. Then soundspeed anomaly $\Delta c/c$ is integrated over the path Γ. For flow of a similar size, measured in v/c, the integration has to be done for $v \cos \mu/c$, where μ is the angle between the path and the flow velocity. There is the reduction factor $|\cos \mu|$ but if integrated over theta (see Averaging below), by rotating ray path, and if we optimize the signal, the integrated reduction factor would be just $2/\pi$.

2. Uncertainty: calculate the uncertainty in travel time obtained for a given pair. If the pair is close to the disc centre, it is known that the so-called realization noise, caused by stochastic excitation, is the dominant source of contribution. Closer to the limb, however, and particularly if the oscillation measurement is done in Doppler, granulation noise can be important. Other quantities that are of importance to uncertainty are spatial resolution, cadence and length of observations.

The way a poor spatial resolution degrade the travel-time measurement, for example, is not through a straightly enhanced statistical uncertainties, which in fact would generally be decreased. When a group of travelling wave packets is measured with a poor resolution, there would be many components travelling between a given pair of pixels, with widely different travel time. As the dispersion in the travel time increase, the travel time between the pixels becomes increasingly ill-defined and therefore difficult to measure.

3. Averaging: Most of the time, a single measurement for just a pair of point is unlikely to yield sufficient signal-to-noise ratio. The averaging may be done in space, or in direction. To account of the effect of averaging we need to know error correlation between quantities that are (probably weighted-)summed.

A note on the direction average -- this is averaging the signal over a ray path that is rotated around the target point. Part of the averaging is about averaging product of projection factor for the pair of surface points where the individual ray begins and ends. As is seen in Figure 31, for annuli of the moderate size, it is adequate to approximate this by squaring the projection factor for the mid point (the surface point directly above the target), or a certainly point close by.

On the other hand, one can produce a fairly robust argument for the inclination requirement by limiting the objective to detection of meridional flow. The meridional flow velocity below 60° degree latitude has been measured by SOHO/MDI. From 30° latitude, therefore, one would be able to measure meridional flow up to the pole, one might think. It is true that from 30° latitude we

observe a surface element at the pole as well as we would a surface element at 60° latitude from the ecliptic plane. As has already been mentioned in the above, however, there is an issue of averaging. The result obtained by Giles et al (1997) was produced by a longitudinal average within 50° from the central meridian. With the increasing latitude μ, the amount of averaging one can carry out would decrease as cos μ even if we keep the longitudinal resolution, which we will not. Let us say we would like to do at 80° latitude as well as SOHO/MDI did at the 60° latitude. By noting $(\cos(60°)/\cos(80°)^{1/2} \sim 1.7$, we can conclude that we will fall short by a factor of at least 1.7; going to 30° latitude may not be enough for measuring meridional flow close to the pole.

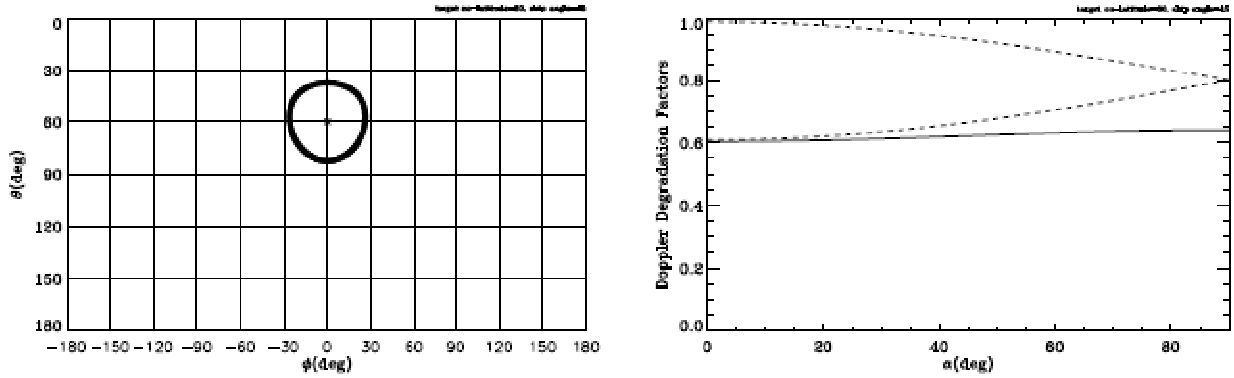

Figure 31. (left:) The path of ray-path end points when a ray with the skip angle of 45, centered around a point at 30 latitude(60 co-latitude) is rotated. (right:) The projection factors at the end points (dashed) as function of , the angle of the path to the local meridian, and its product which is nearly constant (solid)

Appendix B: Jupiter Option

Jupiter option that is described in Section 3.2 cannot reach high latitudes before the solar maximum near the early 2020's. However, the option gives an opportunity to go to high latitudes within current technology if the kick-motor for H-IIA launch vehcle is availabe. When a longer mission duration than the current Jupitor option is acceptable, there are solutions of spacecraft orbit with a higher inclination. The Jupiter option whose final orbit is similar to that of the SEP option in Sections 3.2 and 3.3 is briefly inroduced here.

B.1 Orbit Trajectory

Figure 32 shows the orbit trajectory for the Jupiter option that satisfy both the short cruise time and the maximum orbit inclination. This is essentially a balistic orbit using conventional technology. Minimum distance to the Jupiter is ~60 R_J, so that the radiation environment near the Jupiter is not severe.

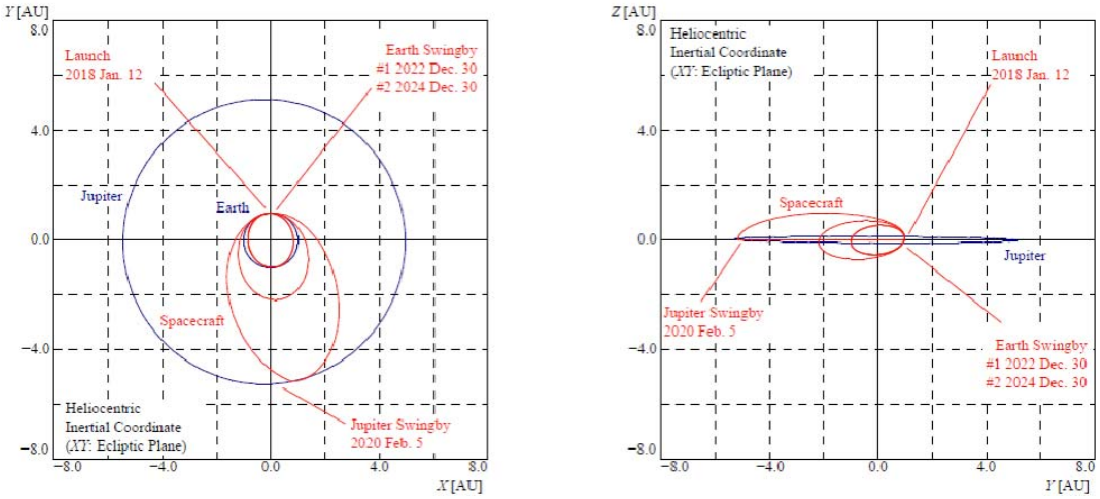

Figure 32. Trajectory profile of Jupiter option

B.2 Mission Profile

The sequence of events of Jupiter option is shown in Table 12. In this sequence, one Jupiter swingby and two Earth swingby operations form the final circular orbit of 1 AU distance from the Sun. A similar orbit is possible for the launch opportunity every ~1.1 year but the maximum orbit inclination is slitly diferent. In the case of 2019 launch, the maximum orbit inclination to the solar ecliptic plane is 36.6°

Table 12. Sequence of events of Jupiter Option

Date	Event	v_∞	i_{SEQ}
2018/01/12	Launch	8.9 km/s	7.1°
2020/02/05	Jupiter Swingby	7.3 km/s	31.4°
2022/12/30	Earth Swingby	17.0 km/s	35.6
2024/12/30	Earth Swingby	17.0 km/s	39.5°

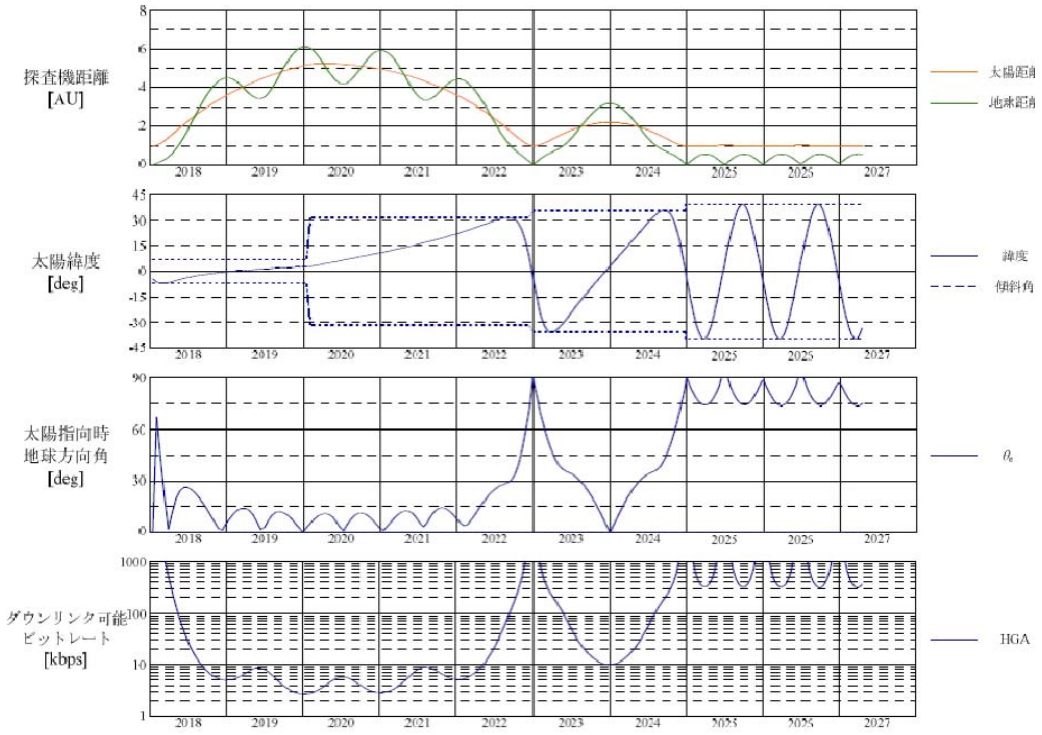

Figure 33. Mission profile of Jupiter option (to be replaced into English version)

Figure 33 shows the mission profile of Jupiter option. This indicates that the first high-data rate observations starts > 4.5 years after the launch. It takes 7 years to reach the final orbit.

B.3 Mass and Power Budget

The mass and power budget are shown in Table 13 and Table 14, respectively.

Table 13. Spacecraft mass budget of Jupiter Option

Component		Mass (kg) Total	Commnent
Mission		130.0	
	Payload	130.0	Tentative allocation
Spacecraft bus		522.5	
	Communication System	94.8	
	Power Control System	142.6	
	Attitude Control System	79.9	
	Chemical Propulsion System	45.8	
	Electrical Propulsion System	0.0	No ion engine this case
	Structure	107.1	
	Thermal Control System	11.6	
	Harness	34.0	
Total dry mass		652.5	
	Fuel	100.0	
	Chemical Fuel	100.0	Scaling from HAYABUSA
	EPS Fuel	0.0	No ion engine this case
Total wet mass		752.5	
Margin		17.5	
Total		770.0	

Table 14. Spacecraft power budget of Jupiter option

Item	Power (W)	
	Near Jupiter	1 AU from Sun
Mission payload	α (TBD; heater)	150
Data hadling system	21.8	21.8
Communication system	79.0	211.3
Power supply system	37.0	51.0
Attitude control system	99.0	106.7
Chemical thruster system	250.0	4.0
Total Power	486.8+α	544.8

Appendix C: References

Belcher, J. W. & Davis, L. 1971, JGR, 76, 3534
Cirtain, J. et al. 2007, Science,
Cranmer, S. R. et al. 1999, ApJ, 511, 481
Dikpati, M. and Gilman, P. A. 2006, ApJ, 649, 498
Forbes, T. G. 2000, JGR, 105, 23153
Gabriel, A. H., 1971, Solar Phys., 21, 392
Giles, P. M., Duvall Jr, T. L., Scherrer, P. H. & Bogart, R. S. 1997, Nature, 390, 52
Haber, D. A. et al. 2002, ApJ, 570, 855
Harrison, R. A. et al. 2009, Solar Phys., 256, 219
Kamio, S. et al. 2009, A&A, 502, 345
Knaack, R. et al. 2001, A&A, 376, 1080
Kohl, J. et al. 1980, ApJ, 241, L117
Kohl, J. et al. 2006, Astron. Astrophys., Rev., 13, 31
Leighton, R. B. et al. 1962 ApJ, 135, 474
Lockwood, G. W., Skiff, B. A., Baliunas, S. L., and Radick, R. R. 1992, Nature, 360, 653
Lockwood, G. W., Skiff, B. A., and Radick, R. R. 1997, ApJ, 485, 789
McComas, D. J. et al. 2003, GRL, 30, 1517
McComas, D. J., Ebert, R. W., Elliott, H. A., Goldstein, B. E., Gosling, J. T., Schwadron, N. A., and R. M. Skoug, R. M. 2008, GRL, 35, L18103
Nakagawa, A. 2007, ApJ, 660, 1660
Parker, E. N, 1965, Planet Space Sci., 13, 949
Radick, R. R., Lockwood, G. W., Skiff, B. A., and Baliunas, S. L. 1988, ApJS, 118, 239
Raouafi, N. E. and Solanki, K. 2006, A&A, 445, 735
Reames, D. V. 1999, Space Sci. Rev., 90, 413
Richardson, I. G. and Cane, H. V. 2004, GRL, 31, L18804
Sheeley, Jr., N. R. Et al. 1997, ApJ, 484, 472
Suzuki, T., and Inutuka, S. 2005, ApJ, 632, L49
Thomas, R. 2003, SPIE, 4853, 417
Thompson, M. J. et al. 1996, Sci, 272, 1300
Tsuneta, S., et al. 2008, ApJ, 688, 1374
Vorontsov, S. V. 2002, Sci, 296, 101
Waldmeier, M., Die Sonnenkorona, Vol. 2, Verlag Birkhäuser 1957.

Appendix D: Acronyms

ACE	Advanced Composition Exploler (spacecraft)
ACS	Attitude Control System
AR	Active Region
ARD	Aerospace Research and development Directorate
BAT	Battery
CCD	Charge Coupled Device
CFRP	Carbon Fiber Reinforced Plastic
CH	Coronal Hole
CIR	Co-rotation Interaction Region
CME	Coronal Mass Ejection
CMOS	Complementary Metal Oxide Semiconductor
CZ	Convection Zone
DHU	Data Handling Unit
DIM	Direct Inclining Method
DPCM	Differential Pulse Code Modulation (,a type of digital communications method)
DSN	Deep Space Network
EAI	EUV Activity Imager proposed for SOLAR-C Plan-A
EDVEGA	Electric Propulsion Delta-V Earth Gravity Assist
EGA	Earth Gravity Assist
EIS	EUV Imaging Spectrometer (on Hinode spacecraft)
EM	Engineering Model
ESA	European Space Agency
ESS	EUV Scanning Spectrometer proposed for SOLAR-C Plan-A
EUV	Extreme UltraViolet
EUVI	EUV Imager (on STEREO spececrafts)
FOV	Field Of View
FWHM	Full Width at Half Maximum
GCR	Galactic Cosmic Rays
GONG	Global Oscillation Network Group (by observing the Sun with six ground-based observatories for helioseismology)
HAI	Helioseismic Activity Imagier proposed for SOLAR-C Plan-A
HCE	HouseKeeing Electronics
HK	HouseKeeping
HMI	Helioseismic Magnetic Imager (on Solar Dynamics Observatory)
HS	HelioSeismology
ICME	Interplanetary Coronal Mass Ejection a type of digital communications method
IEM	Ion Engine Module
IES	Ion Engine System
IHI	Inner Heliospheric Imager proposed for SOLAR-C Plan-A
IPM	IES Pointing Mechanism
IPS	InterPlanetary Scintillation
IPU	IES Power Unit
ISAS	Institute of Space and Astronautical Science
ISP	SPecific Impulse
ITA	Ion Thruster Assembly

ITCU	Ion Thruster Control Unit
JAXA	Japanese Aerospace Exploration Agency
JGA	Jupiter Gravity Assist
JPEG	Joint Photographic Experts Group (, a group which created a data compression)
JPL	Jet Propulsion Laboratory
LASP	Laboratory for Atmospheric and Space Physics
LIM	Luminosity and Irradiance Monitor proposed for SOLAR-C Plan-A
MDI	Michelson Doppler Imager (on SOHO)
MHD	Magneto-HydroDynamics
MLI	Multi-Layer Insulator
MMO	Mercury Magnetospheric Orbiter
MSU	Microwave Supply Unit
NAOJ	National Astronomical Observatory of Japan
NASA	National Aereopace Agency
PCU	Power Control Unit
PMOD	Physikalisch-Meteorologisches Observatorium Davos
PMU	Propellant Management Unit
PREMOS	PREcision MOnitor Sensor on PICARD spacecraft for monitring TSI
PYC	Pyrotechnic Controller
QS	Quiet Sun
RW	Reaction Wheel
RZ	Radiative Zone
SAP	Solar Array Panel
SDO	Soalr Dynamics Observatory (spacecraft)
SEM	Sequential EDVEGA Method
SEP	Solar Energetic Particle in science part or Solar Electric Propulsion in engineering
SOHO	Solar and Heliospheric Observatory (spacecraft)
SORCE	SOlar Radiation and Climate Experiment (spacecraft)
SOT	Solar Optical Telescope on Hinode spacecraft
SSR	Serieis Switching Regulator
STEREO	Solar TErrestrial RElations Observatory (spacecrafts)
TCIM	Telemetry Command Interface Module
TIM	Total Irradiance Monitor (on SORCE)
TR	Transition Region
TRL	Technical Readiness Level
TSI	Total Solar Irradiance (on SORCE spacecraft)
UV	UltraViolet
UVCS	UltraViolet Coronagraph Spectrometer (on SOHO)
VGA	Venus Gravity Assist
VIRGO	Variability of solar IRradiance and Gravity Oscillations (on SOHO)
XRT	X-Ray Telescope (on Hinode spacecraft)